IRSTI 41.25.31; 41.25.19; 41.25.29 https://doi.org/10.26577/phst202613110

# Identification of young star objects in the serpens south star-forming region of the aquila molecular cloud

N.Sh. Alimgazinova [1,2], A.B. Manapbayeva [2,3], A.Zh. Omar [1,2*], K.M. Turekhanova [1,2], N.E. Abildayev [4], A. Demessinova [1,2], A.A. Alibek [3] and N.B. Shaimoldin [5]

[1]Faculty of Physics and Technology, Farabi University, Almaty, Kazakhstan
[2]Institute of Experimental and Theoretical Physics, Farabi University, Almaty, Kazakhstan
[3]Kazakh National Women's Teacher Training University, Almaty, Kazakhstan
[4]Faculty of Mechanics and Mathematics, Farabi University, Almaty, Kazakhstan
[5]State Key Laboratory of Radio Astronomy and Technology,
Xinjiang Astronomical Observatory, CAS, Urumqi, Xinjiang, P. R. China
*e-mail: omar.aruzhan@kaznu.kz
*(Received November 6, 2025; received in revised form May 20, 2026; accepted May 25, 2026)*

We present the results of a search and identification of young stellar objects (YSOs) in the Serpens South star-forming region, which is part of the Aquila Rift complex. Using AllWISE catalog data within a radius of 7′ from the center of the region, a multi-stage filtering procedure was applied to remove contaminating sources, including galaxies, active galactic nuclei, shock emission sources and PAH emission. Photometric criteria were then used to classify the sources according to their evolutionary stages. As a result, a sample of 145 YSO candidates was identified, including 1 protostar, 37 Class I objects, 48 Class II objects, 47 Class III objects and 12 transition disks. A quantitative analysis of the spatial distribution of the sources was performed using cumulative distribution functions, the Kolmogorov–Smirnov test and bootstrap resampling. The results show that early-stage objects (Class I) exhibit pronounced clustering in the central region ($R_{50}$ = 0.26 pc) and are associated with dense filamentary structures, whereas Class II and III objects display a more extended distribution. A Jeans analysis combined with Monte Carlo simulations yielded a median gas density of $n \approx 1.6 \times 10^5$ cm$^{-3}$, consistent with dense prestellar cores. Multiwavelength verification using infrared, X-ray, optical and radio catalogs showed that 78.6% of the objects possess independent infrared confirmation, while 70.3% have X-ray detections. In addition, 11 new YSO candidates not previously reported in published catalogs were identified. The obtained results demonstrate the high efficiency of WISE data for detecting heavily obscured sources and provide new insights into the early stages of star formation in dense filamentary environments.

**Keywords:** Young stellar objects, Serpens South, Aquila Rift, WISE, star formation.

## 1. Introduction

The study of star formation and stellar evolution remains one of the central problems of modern astrophysics, since stars play a fundamental role in the formation and dynamical evolution of galaxies. In this context, star-forming regions are of particular importance, as they provide an opportunity to investigate the early stages of stellar evolution and the spatial distribution of young stellar objects (YSOs).

Observations of young stars embedded in molecular clouds are significantly hindered at optical wavelengths because of strong extinction caused by interstellar dust [1]. Infrared observations provide an effective way to overcome this limitation by revealing sources with infrared excess emission associated with circumstellar disks and envelopes. Major advances in this field have been enabled by the Spitzer Space Telescope [2] and the Wide-field Infrared Survey Explorer (WISE) mission [3], which provided extensive infrared photometric surveys that form the basis of modern YSO identification techniques.

The classification of YSOs [4–10] is commonly performed using two principal approaches: infrared color diagnostics and the spectral index α, which characterizes the slope of the spectral energy distribution. Infrared color criteria are widely used in the analysis of large infrared surveys, allowing efficient identification of YSO candidates while simultaneously removing a significant fraction of background contaminants [11–14]. At the same time, classification based on the spectral index provides a physically motivated separation of sources into evolutionary classes (Class I, II and III) [15]. In the present work, we primarily focus on photometric classification based on infrared colors using modern criteria for contaminant rejection and sample purification.

The Serpens South star-forming region, which is part of the Aquila Rift complex, is an active environment characterized by a high concentration of young stellar objects and a pronounced filamentary structure [16–19]. Despite the availability of high-angular-resolution observations obtained with facilities such as *Spitzer* and *Herschel*, the WISE catalog remains an important resource because of its full-sky coverage and the uniformity of its photometric data, which are particularly valuable for statistical analyses and cross-matching studies.

In contrast to studies aimed at constructing large-scale YSO catalogs across extended sky regions using uniform selection criteria [20], this work focuses on a detailed investigation of the local Serpens South star-forming region. Such a localized analysis makes it possible to examine how environmental factors, including extinction, gas density and the evolutionary state of the molecular cloud, influence the observed properties of the YSO population [21].

A comprehensive source-selection procedure was implemented, combining successive contaminant removal with multi-stage verification of YSO candidates using data from 19 astrophysical catalogs covering the infrared, X-ray, radio and optical wavelength ranges. In addition, statistical techniques and numerical simulations were employed to study the spatial distribution of YSOs belonging to different evolutionary classes, enabling an assessment of their clustering behavior and its relation to the physical characteristics of the surrounding medium.

The adopted methodology resulted in the identification of previously uncataloged YSO candidates and allowed us to investigate the connection between their spatial distribution and evolutionary properties. These results provide additional constraints on the physical conditions and dynamical state of the star-forming environment in the Serpens South region.

## 2. Observations

The Aquila molecular cloud complex, also known as the Aquila Rift, is a prominent dark-cloud structure located in the constellations Aquila, Serpens Cauda and Ophiuchus. It consists of extended interstellar dust and molecular clouds distributed along a large northeast–southwest elongated feature. The Aquila Rift forms part of the Great Rift, a nearby system of dark clouds whose dust obscures the central regions of the Galactic plane and the inner sectors of the Milky Way.

Several active star-forming regions are located within the western part of the Aquila Rift, including Serpens Main, Serpens South, W40 and MWC297. CO and HI observations [22, 23] show that the complex extends along the Galactic plane over Galactic longitudes from approximately 20° to 40° and Galactic latitudes from about −1° to 10°. However, the relative distances between the embedded protoclusters Serpens South and W40 remain uncertain. Whether the Aquila Rift and the main Serpens cloud belong to the same molecular complex and therefore share a common distance is still under discussion [24, 25].

Previous studies have suggested that Serpens Main and the Aquila Rift may represent physically distinct structures, which could explain the discrepancy between their estimated distances [26, 27]. In particular, distance estimates of approximately 200–280 pc have been reported for the Aquila Rift complex, whereas Serpens Main is commonly placed at a distance of about 415 pc, implying that Serpens Main is located farther away than Serpens South. More recent studies focused on the Serpens South protocluster [28] adopted a distance of approximately 260 pc for this star-forming region.

Based on extinction measurements [29] and radio spectral-line observations [30, 31], the nearby H II region W40 has generally been placed at distances ranging from about 300 to 700 pc. A more recent Chandra X-ray study [32], based on X-ray luminosity function arguments, suggested that the most probable distance to the W40 cluster is approximately 600 pc, although a smaller distance of about 300 pc could not be excluded.

Among the star-forming regions associated with the Aquila Rift cloud complex, Serpens South is of particular interest. Serpens South is a young embedded cluster discovered through infrared observations with *Spitzer*. The cluster is embedded within a dense filamentary molecular cloud containing a large population of protostars. Owing to the high concentration of protostars and prestellar cores in this region, Serpens South is considered one of the most active sites of star formation within the Aquila Rift complex (Figure 1). Large-scale magnetic fields have been detected in the region, oriented predominantly perpendicular to the main cloud filament, whereas several sub-filaments tend to align parallel to the primary filamentary structure. Such magnetic fields may play an important role in slowing the gravitational collapse of dense molecular condensations within the complex.

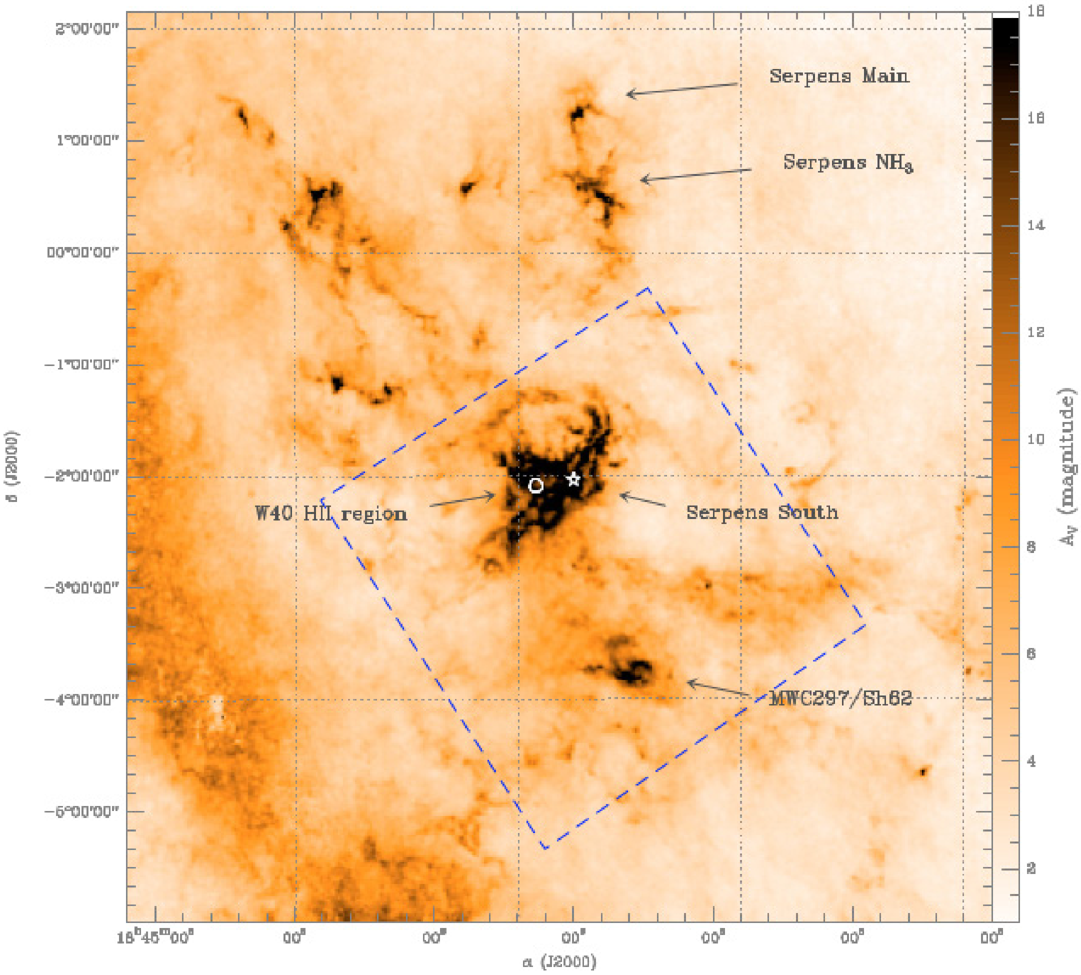


**Figure 1.** Aquila Rift/Serpens region based on 2MASS observations [16].

*Spitzer* observations show that W40 and the embedded Serpens South cluster are located close to each other on the plane of the sky, suggesting that Serpens South may be physically associated with the more evolved W40 region. Recent distance measurements for Serpens Main and W40 yielded values of approximately 436 pc, implying that Serpens South may be located at a similar distance because the two regions appear to be kinematically connected. Studies by [33, 34] estimated the mass of the giant molecular cloud associated with W40 to be approximately ~1.4 × $10^5$ $M_\odot$ and derived a characteristic distance of about 474 pc. Similarly, it has been suggested that Serpens South may interact with the expanding shell of the W40 H II region, further supporting the possibility that the two regions are located at nearly the same distance. However, large-scale observations of the $^{12}$CO (2–1) and $^{13}$CO (2–1) emission toward the Aquila Rift revealed two spatially extended components associated with Serpens South and W40 that exhibit different radial velocities. These results suggest that large-scale expanding shells, bubbles and/or gas flows influence the observed velocity fields and may play an important role in the formation and evolution of these molecular clouds [35].

As part of the Herschel Gould Belt Survey [36], a 3.3° × 3.3° region toward the Aquila complex was mapped in the far-infrared wavelength range. The resulting maps provide high spatial resolution and sensitivity across five bands between 70 and 500 μm. A large population of previously unidentified protostars and prestellar cores was detected, primarily concentrated within three active star-forming regions: the filamentary molecular cloud hosting Serpens South, the eastern H II region W40/Sh2-64 and the southern MWC 297/Sh2-62 region.

Therefore, the Aquila Rift complex, which contains star-forming regions at different evolutionary stages and physical conditions, represents an important laboratory for investigating the early stages of star formation over a wide range of wavelengths and observational techniques.

### 3. Source Selection and Initial Data Processing

A literature review of nearby star-forming regions was carried out in order to determine their central coordinates, angular sizes and the corresponding search radius required for the identification of young stellar objects (YSOs). The Serpens South region, centered at RA(J2000) = $18^h30^m03^s$ and Dec(J2000) = −02°01′58.2″, has an apparent size of approximately 14.4 × 20.3 arcmin.

The search for YSO candidates was performed using the SIMBAD Astronomical Database (CDS, Strasbourg) and the AllWISE Data Release catalog [37]. For the Serpens South region, a search radius of 7 arcmin was adopted within the coordinate range 277.39° ≤ α ≤ 277.62° and −2.031° ≤ δ ≤ −2.036°. A total of 682 infrared sources were identified within this area. The detected source density is consistent with the expected infrared source population toward this portion of the Galactic plane and includes both potential YSO candidates and a significant number of background and extragalactic contaminants.

An initial photometric quality filtering was applied to the Serpens South dataset in order to exclude sources with unreliable flux measurements. Only objects with photometric uncertainties smaller than 0.2 mag were retained. This threshold provides a balance between sample completeness and photometric reliability by removing low signal-to-noise detections, consistent with approaches commonly adopted in similar studies. At the same time, it should be noted that this criterion may exclude a fraction of faint but physically real sources.

For the subsequent analysis, only sources with non-zero magnitudes in all four WISE bands (W1, W2, W3 and W4) were considered. For convenience, the following color-index notation was adopted throughout this work: W1-W2 by $W_{12}$; W2-W3 by $W_{23}$; W1-W3 by $W_{13}$, W2-W4 by $W_{24}$ и W3-W4 by $W_{34}$.

The next stage of the analysis involved the removal of contaminating sources that may exhibit infrared colors similar to those of YSOs. The first class of contaminants consists of star-forming galaxies. Galaxies undergoing active star formation typically show enhanced polycyclic aromatic hydrocarbon (PAH) emission produced through interactions between interstellar dust and ultraviolet radiation fields.

Star-forming galaxies dominated by polycyclic aromatic hydrocarbon (PAH) emission typically exhibit very red infrared colors, characterized by large values of W23 and are generally fainter than typical young stellar objects. In this study, we adopted the same approach based on established color-selection criteria. The criteria used to identify and remove probable star-forming galaxies were: $W_{23}>1$; $W_{12}<1$; $W_{12}<0.46\cdot W_{23}-0.466$ and W1>12 (or W2>11). All criteria were required to be satisfied simultaneously in order to reliably identify contaminating sources. Applying these conditions to the Serpens South region resulted in the identification of 5 infrared sources associated with star-forming galaxies. The adopted selection criteria are based on characteristic infrared colors related to PAH emission and are widely used in similar studies, confirming their effectiveness for separating extragalactic contaminants from YSO candidates.

Another important class of contaminants consists of active galactic nuclei (AGNs), whose mid-infrared fluxes may closely resemble those of young stellar objects. AGN emission is generally fainter than that of typical YSOs in regions located within approximately 5 kpc. Since the studied region is located at a distance of less than 1 kpc, these selection criteria are particularly important for the present sample. The criteria adopted to identify and remove probable AGNs were: $W1>1.8\cdot W_{13}+4.1$ and W1>13 (or W2>12, or $W1> W_{13}+11$). Applying these criteria to the Serpens South region resulted in the identification of 211 infrared sources consistent with AGN contamination. It should be noted that, despite the application of strict selection criteria, some AGNs may still remain within the sample because of the overlap between their photometric properties and those of young stellar objects, representing one of the main sources of uncertainty in the classification process.

In addition to star-forming galaxies and AGNs, infrared emission may also arise from shocked gas structures and polycyclic aromatic hydrocarbon (PAH) emission associated with the interstellar medium. The criteria adopted for removing these Galactic contaminants were based on their characteristic infrared colors. Shock-emission sources were identified using the color criteria $W_{12}>1$ and $W_{23}<2$. Applying these conditions to the Serpens South region resulted in the identification of 40 shock-emission sources. The relatively large number of such sources supports previous evidence for active motions of interstellar material within the region. To exclude PAH-emission sources, two sets of color criteria were applied: first, $W_{12} < 1$ and $W_{23} > 4.9$ and second, $W_{12} < 0.25$ and $W_{23} > 4.75$. Using these conditions, 17 PAH-emission sources were identified in the Serpens South region. The removal of these types of contaminants represents an important step in the analysis, since diffuse interstellar emission and shocked structures may mimic the infrared characteristics of young stellar objects, particularly in active star-forming environments.

For the investigated Serpens South region, the application of all photometric quality and color-selection criteria resulted in the exclusion of 273 out of 496 infrared sources as potential contaminants, including galaxies, active galactic nuclei, PAH-emission sources and shock-related structures. Such a high contamination fraction is a common characteristic of wide-field infrared surveys such as WISE, where extragalactic sources and diffuse interstellar structures may reproduce the photometric properties of young stellar objects.

To improve the reliability of the results, an additional assessment of photometric quality was performed using the AllWISE catalog flags [38]. Only sources with quality flags A and B, corresponding to signal-to-noise ratios of $w_{SNR} > 3$, were included in the analysis, ensuring sufficient photometric accuracy in the infrared bands. Nevertheless, even sources satisfying these criteria may still be associated with diffuse interstellar emission, particularly in the W3 (12 μm) band, where the background contribution becomes significant. Therefore, all candidates were additionally inspected visually using W3 images and combined W1–W3 maps, following approaches commonly adopted in studies of star-forming regions. Sources that did not exhibit a clear point-like morphology in the W3 band or were associated with diffuse structures were excluded from further analysis [39].

After all stages of filtering, the final sample consisted of 148 sources, corresponding to approximately 29.8% of the initial sample. Although photometric classification based on infrared criteria inevitably retains some degree of uncertainty because of the limited spatial resolution of WISE data and the partial overlap between the color properties of different source populations, the applied filtering procedure substantially reduces contamination and provides a statistically reliable sample of probable young stellar object candidates suitable for further analysis.

## 4. Results and discussion

### *4.1 Identification of young stellar objects*

In this study, the identification of YSOs was performed using WISE photometric criteria combined with a classification scheme supplemented by 2MASS data. The inclusion of near-infrared measurements makes it possible to refine the classification boundaries and reduce the overlap between the color distributions of different source populations, thereby improving the robustness of the method and reducing the probability of false classifications.

Additional selection criteria involving fluxes in all four WISE bands (W1–W4) were applied for the identification of protostars, allowing a more reliable separation from extragalactic contaminants, including active galactic nuclei (AGNs). As a result, 2 protostar candidates were identified in the Serpens South region. Their presence is supported by previous infrared observations, particularly *Spitzer* Gould Belt Survey data, which revealed a dense embedded cluster of protostars in this region, as well as by far-infrared *Herschel* observations indicating a large population of protostellar and prestellar cores.

The identification of Class I and Class II objects was carried out using WISE color criteria with additional constraints based on 2MASS data. In total, 37 Class I objects and 48 Class II objects were identified. In addition, 12 sources were classified as transition-disk objects, while 49 sources were assigned to Class III.

Based on the resulting classification, a color–color diagram ($W_{12}$ versus $W_{23}$) was constructed for all identified YSO candidates (Figure 2). The dashed lines indicate the classification boundaries separating different evolutionary stages of YSOs. The horizontal boundary at $W_{12} = 0.25$ defines the lower limit of infrared excess, whereas the vertical boundary at $W_{23} = 2.0$ separates more deeply embedded sources with enhanced mid-infrared emission.

The distribution of sources on the diagram demonstrates a clear evolutionary sequence. Class I objects are concentrated in the region of large color indices, consistent with the presence of dense dusty envelopes. Class II objects occupy an intermediate region associated with protoplanetary disks, while Class III objects and transition disks are located closer to the photospheric region, reflecting the reduced infrared excess at later evolutionary stages. One protostar is located in the region of high W12 values, indicating the presence of a dense cocoon-like envelope of gas and dust. Although its color index is lower than that of some Class I objects, it remains significantly separated from the photospheric and Class II regions, supporting its classification as one of the youngest and most deeply embedded objects in the sample.

During the analysis, several sources with anomalous color indices were identified, including objects with negative values of W23 or W12. Such values are inconsistent with the expected infrared properties of dusty envelopes and are most likely associated with the sensitivity limitations of the WISE telescope, particularly in the W3 band, as well as with contamination from diffuse background emission. In total, 3 anomalous sources out of 148 (≈2.0%) were identified. The complete list of anomalous objects is provided in Appendix A.

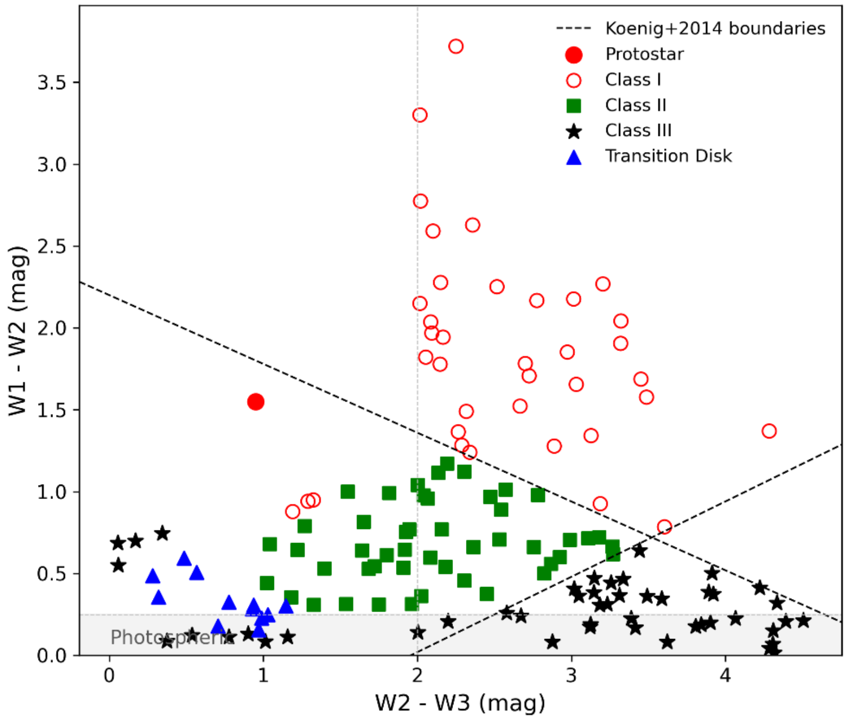


**Figure 2.** WISE color–color diagram (W1−W2) vs. (W2−W3) for young stellar object candidates in the Serpens South region.

The presence of these anomalous sources reflects residual photometric uncertainties and does not significantly affect the overall distribution of the sample. The relatively low fraction of anomalous objects (~2%) indicates the high purity of the final sample and confirms the effectiveness of the adopted filtering procedure.

Thus, the constructed color–color diagram reflects the distribution of reliably identified sources and confirms the validity of the adopted classification criteria, while also demonstrating the evolutionary structure of the young stellar object population in the Serpens South region.

*4.2 Spatial distribution of young stellar objects*

*a) Spatial distribution map of young stellar objects*

To investigate the structural relationship between YSOs at different evolutionary stages and the surrounding interstellar medium, a spatial distribution map of YSOs in the Serpens South region was constructed. Figure 3 presents the identified YSO candidates overlaid on a WISE 12 μm infrared image. Such a visualization makes it possible to examine the degree of concentration of the youngest objects, including protostars and Class I sources, along the dense gas-and-dust filaments of the nebula, as well as to trace the evolutionary segregation process, in which stars gradually disperse as they evolve from deeply embedded protostellar cores into more evolved Class III systems.

Figure 3a shows the spatial distribution of Class I objects, Class II objects, transition disks and protostars. Sources at the earliest evolutionary stages, including protostars and Class I objects, exhibit a pronounced concentration toward the central region, spatially coinciding with the densest and most highly obscured structures visible in the infrared map. Such a distribution is characteristic of young protostellar populations closely associated with dense molecular filaments [40]. Class II objects display a more extended distribution, occupying both the central and peripheral regions, indicating a more advanced evolutionary stage and partial dynamical relaxation [41]. Transition-disk objects do not exhibit a strong central concentration and are predominantly distributed at intermediate and larger distances from the cluster center, consistent with their interpretation as more evolved systems. It should be noted that the protostar sample in the present study is limited (N = 1), preventing statistically significant conclusions regarding their spatial distribution.

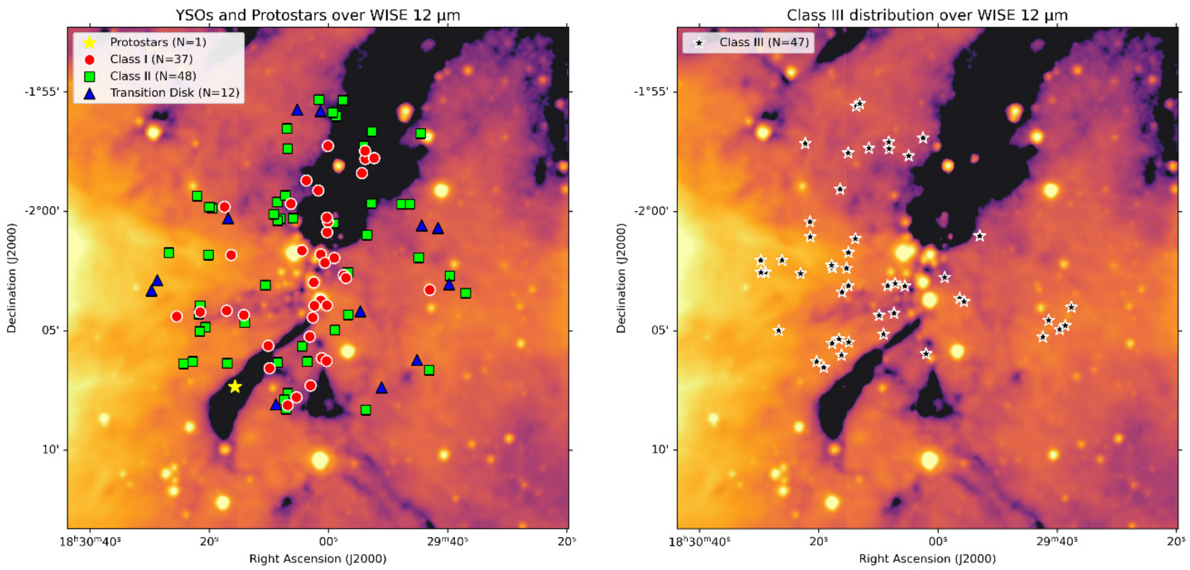


*(a) YSO candidates: protostar, Class I and Class II objects and transition disks*

*(b) Class III YSO candidates*

**Figure 3.** Spatial distribution of YSO candidates of different evolutionary classes in the Serpens South region overlaid on the WISE 12 μm map.

The observed spatial distribution of different YSO classes reflects an evolutionary sequence in which younger objects remain closely associated with dense molecular-cloud structures, whereas more evolved sources gradually disperse as a result of cluster dynamical evolution and interactions with the surrounding environment. Similar behavior has previously been reported in several star-forming regions, including Serpens South and Orion.

Figure 3b shows the spatial distribution of Class III YSO candidates in the Serpens South region. In contrast to younger objects, Class III sources exhibit a significantly more uniform and extended spatial distribution, without a pronounced concentration toward the central part of the region. Such a distribution is consistent with the expected dynamical evolution of stellar clusters, in which Class III objects, having lost their protoplanetary disks, represent a more evolved population that has had sufficient time to migrate away from their formation sites. The absence of a clear correlation with dense infrared structures further indicates that these objects are no longer directly associated with active star-forming regions, in agreement with observations of other star-forming environments.

*b) Radial properties of YSO candidates of different evolutionary classes*

To quantitatively investigate the spatial distribution of YSO candidates in the Serpens South region, radial distances relative to the cluster center were analyzed. Source coordinates were obtained from the AllWISE catalog and converted into equatorial coordinates (J2000) expressed in degrees. The cluster center was defined using the median coordinates of the Class I objects. This choice is motivated by the fact that Class I sources correspond to the earliest evolutionary stages and are therefore expected to remain spatially associated with ongoing star formation. The use of median values instead of mean coordinates reduces the influence of asymmetries and outliers in the spatial distribution.

Radial distances were calculated under the small-angle approximation with a cosine correction applied to declination $r = \sqrt{(\Delta cos\delta\ )^2 + (\Delta\delta)^2}$, where Δα and

Δδ represent the offsets in right ascension and declination relative to the cluster center and r is expressed in arcminutes [42].

To compare the spatial distributions of different evolutionary classes (Class I, II, III and transition-disk YSO candidates), cumulative distribution functions (CDFs) were used, thereby avoiding dependence on binning and enabling robust comparisons between samples of different sizes [43]. For each class, an empirical cumulative distribution function of radial distances was constructed. The statistical significance of the differences between distributions was evaluated using the Kolmogorov–Smirnov test, which measures the maximum deviation between two empirical cumulative distributions and estimates the probability that the samples originate from the same parent distribution. In addition, mean and median radial distances were calculated for each class and used as independent indicators of spatial concentration.

To evaluate the robustness of the median values, a bootstrap resampling procedure was applied [44]. For each sample, 5000 bootstrap realizations with replacement were generated, allowing the distribution of median radii and the corresponding 68% confidence intervals to be determined. This procedure is particularly important for the relatively small sample of transition disks (N = 12), for which standard statistical estimates may be unstable.

Figure 4 presents the cumulative radial distributions (CDFs) for Class I, II, III and transition-disk YSO candidates relative to the cluster center. The distribution corresponding to Class I objects is systematically shifted toward smaller radii, indicating a high degree of spatial concentration. The median radius for this class is $r_{med}$ = 3.50 arcmin.

The distributions of Class II and III objects are nearly identical and are characterized by median radii of approximately 5.2 arcmin, indicating a more spatially extended structure. This result is supported by the Kolmogorov–Smirnov test, which reveals no statistically significant difference between these classes ($p \approx 0.91$).

Transition disks exhibit a systematic shift toward larger radii, with a median value of $r_{med}$ = 5.46 arcmin. The confidence interval derived from bootstrap resampling (5.38–6.09 arcmin) does not overlap with that of the Class I population, indicating the absence of strong central concentration for transition-disk objects. At the same time, partial overlap with the distributions of Class II and III sources suggests statistical consistency with more evolved populations.

Overall, the obtained results are consistent with the standard evolutionary picture of YSOs, in which younger objects remain concentrated in the central star-forming regions, whereas more evolved sources become distributed over a larger spatial volume.

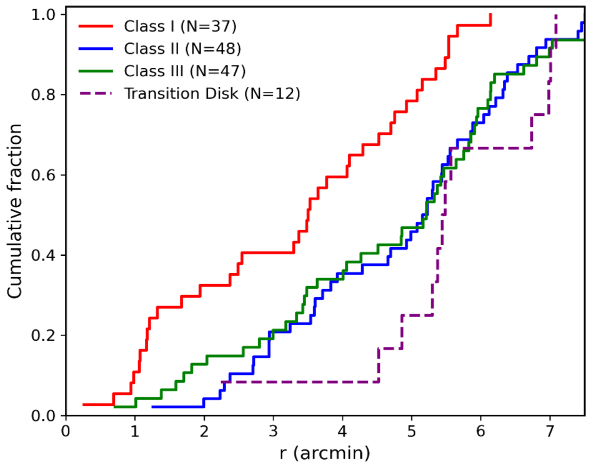


**Figure 4**. Cumulative distribution functions of radial distances for young stellar object candidates of different evolutionary classes in the Serpens South region.

**Table 1.** Radial properties of YSO candidates belonging to different evolutionary classes.

| Class of objects | N | ⟨r⟩ (arcmin) | $r_{med}$ (arcmin) | 68% CI (arcmin) |
|---|---|---|---|---|
| Class I | 37 | 3.27 | 3.50 | 3.30–3.77 |
| Class II | 48 | 4.81 | 5.19 | 4.93–5.31 |
| Class III | 47 | 4.66 | 5.22 | 4.85–5.37 |
| Transition Disk | 12 | 5.55 | 5.46 | 5.38–6.09 |

*c) Quantitative analysis of the spatial distribution of YSOs*

A quantitative analysis of the spatial distribution of young stellar objects at early evolutionary stages in the Serpens South region was further performed, revealing systematic differences between evolutionary classes.

Figure 5 presents the spatial distribution of YSO candidates in the Serpens South region overlaid on the WISE 12 μm infrared emission map together with contour lines corresponding to the kernel density estimation (KDE) of the source distribution [45]. The color map represents the infrared intensity on a logarithmic scale ($MJy/sr^{-1}$). The left panel (Figure 5a) shows the distribution of protostars (yellow stars) and Class I objects (red circles). Regions of enhanced source density, indicated by white contours, demonstrate pronounced clustering, with the sources concentrated along an elongated structure associated with a dense molecular filament. The right panel (Figure 5b) presents the distribution of Class II objects (green squares). Their spatial distribution appears more diffuse, while the density contours (green) indicate significantly weaker clustering compared with the Class I population.

For the early evolutionary classes of YSO candidates, several quantitative spatial parameters were calculated, including R50, the characteristic radius containing 50% of the objects of a given class; NN (Nearest Neighbor), defined as the mean distance to the nearest neighboring source; and KDE (Kernel Density Estimation), corresponding to the peak value of the kernel density distribution. The first parameter characterizes the local concentration of objects, the second describes the compactness of the population and the third reflects the maximum projected surface density of sources within the cluster.

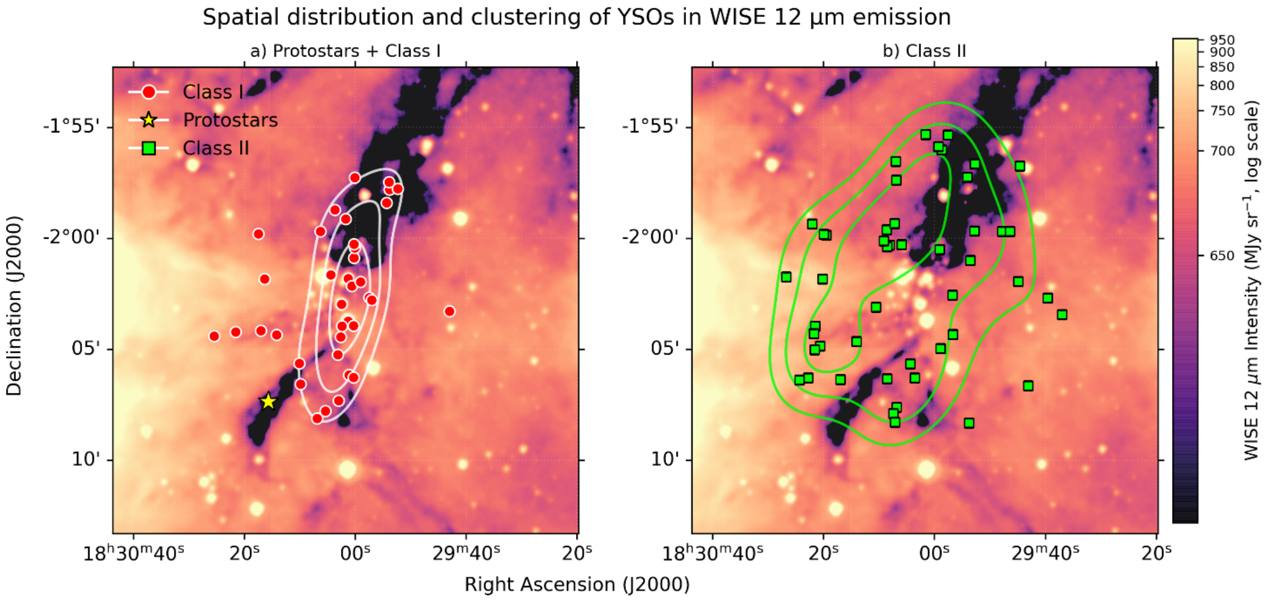


**Figure 5.** Spatial distribution and clustering of YSO candidates based on WISE infrared emission at 12 µm.

Class I objects exhibit a more compact spatial distribution, characterized by a radius of $R_{50}$ = 0.26 ± 0.03 pc, whereas Class II objects show a larger characteristic radius of $R_{50}$ = 0.37 ± 0.02 pc. Thus, the characteristic spatial scale increases by approximately 40% from Class I to Class II sources. The mean nearest-neighbor distance also increases from 0.055 pc for Class I objects to 0.066 pc for Class II objects, indicating a decrease in the local source density. The KDE analysis further shows that the peak density of the Class I population is approximately three times higher than that of the Class II population, implying significantly stronger clustering at earlier evolutionary stages.

Protostars in the present sample are represented by a limited number of objects (N = 1), preventing a statistically meaningful quantitative analysis of their spatial distribution. Nevertheless, their localization within the region of maximum source density is consistent with the expected location of the youngest objects near the centers of active star formation.

The obtained results are consistent with the established evolutionary picture of stellar clusters, in which the youngest objects, including protostars and Class I sources, remain concentrated within dense filamentary structures, whereas more evolved objects, such as Class II and Class III sources, exhibit a more extended spatial distribution.

**Table 2.** Spatial distribution parameters.

| Parameter | Class I | Class II |
|---|---|---|
| Number of objects (N) | 37 | 48 |
| ($R_{50}$) (pc) | 0.26 ± 0.03 | 0.37 ± 0.02 |
| NN (pc) | 0.055 | 0.066 |
| KDE peak | $2.95 \cdot 10^{-5}$ | $1.05 \cdot 10^{-5}$ |

*d) Estimation of the Physical Parameters of the Serpens South Region Using the Monte Carlo Method*

To quantitatively interpret the observed clustering scale of the identified young stellar objects, a Jeans analysis was performed taking into account the uncertainties of the input parameters. The mean nearest-neighbor separation, $L_{obs} \approx 0.06$ pc, was adopted as the characteristic fragmentation scale. The gas temperature was assumed to lie within the range of 10–15 K, corresponding to typical conditions in dense molecular clouds [46]. Since the Jeans length depends nonlinearly on both temperature and density, Monte Carlo simulations were applied in order to obtain a statistically robust estimate of the physical parameters of the environment. Within $10^4$ realizations, the gas temperature and the observed spatial scale were randomly varied and for each realization the gas density satisfying the condition $\lambda_J \approx L_{obs}$ was determined.

The simulation results are presented in Figure 6, which shows the resulting gas-density distribution. The histogram represents the Monte Carlo sample, while the solid curve corresponds to the smoothed kernel density estimation (KDE). The vertical dashed line marks the median value, whereas the dotted lines indicate the 68% confidence interval. The resulting distribution is close to log-normal in shape, with a moderate asymmetry toward higher densities.

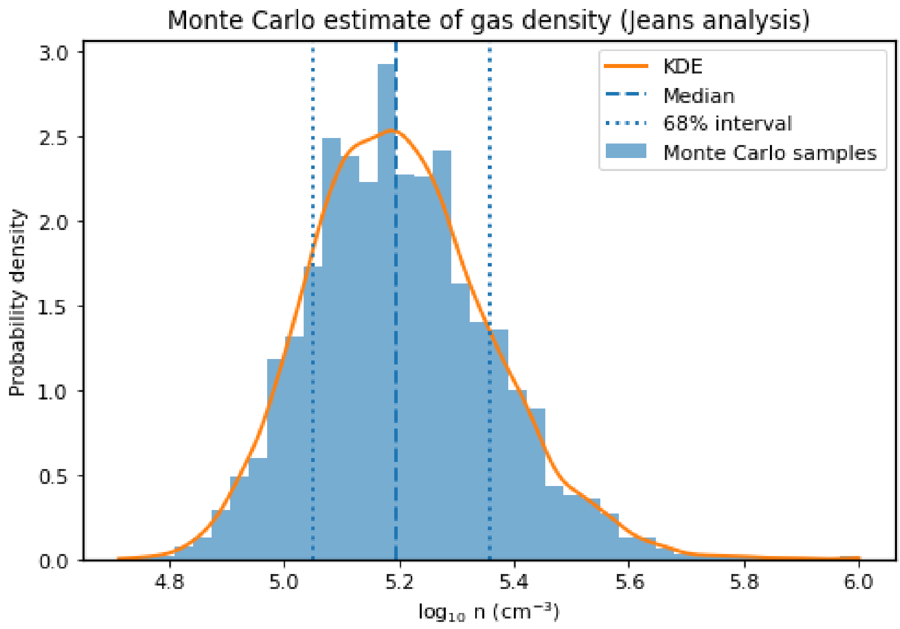


**Figure 6.** Monte Carlo estimation of gas density from Jeans analysis in Serpens South.

The numerical estimates are summarized in Table 3. The median gas density is found to be $n \approx 1.6\times10^5\, cm^{-3}$, with a 68% confidence interval of $n \approx (1.1–2.2)\times10^5\, cm^{-3}$. These values significantly exceed the average density of typical molecular clouds ($\sim 10^3–10^4\, cm^{-3}$) and are consistent with dense filamentary structures and prestellar cores [47]. Previous studies of the Serpens South region have shown that star formation occurs within a dense filamentary structure characterized by a high concentration of protostars [48].

Thus, the obtained results are consistent with the current paradigm of filamentary star formation, in which gravitational fragmentation of dense filaments plays a key role [49]. The observed clustering scale of the YSO candidates corresponds to the Jeans scale within the densest regions of the filaments, confirming the connection between the spatial distribution of the sources and the physical conditions of the surrounding medium.

It is important to note that the contribution of temperature uncertainty to the final result is secondary compared to the effect of gas density, in agreement with theoretical estimates of the Jeans-length sensitivity [50]. This indicates that gas density plays the dominant role in determining the fragmentation scale.

**Table 3.** Estimated gas density parameters.

| Parameter | Value |
|---|---|
| Median ( n ) | $(1.56\times10^5)$ cm$^{-3}$ |
| Mean ( n ) | $(1.71\times10^5)$ cm$^{-3}$ |
| Lower limit (16%) | $(1.12\times10^5)$ cm$^{-3}$ |
| Upper limit (84%) | $(2.24\times10^5)$ cm$^{-3}$ |
| Confidence interval (68%) | $((1.12–2.24)\times10^5)$ cm$^{-3}$ |

*4.3 Multiwavelength verification and comparative analysis of YSO candidates*

To independently verify the adopted classification and evaluate the novelty of the resulting YSO candidate sample in the Serpens South region (1 protostar, 37 Class I objects, 48 Class II objects, 47 Class III objects and 12 transition disks), a multiwavelength cross-identification analysis was performed using 19 astrophysical catalogs and published studies. The analysis included infrared catalogs (7 catalogs, including 2MASS, WISE/NEOWISE, *Spitzer*, as well as the general source catalog and YSO sample presented in [20]), X-ray catalogs (3 catalogs: SFiNCs [51], *Chandra* and MORX [52]), radio [40] and submillimeter catalogs (4 catalogs: VLA GBS [53-55]), as well as combined and optical datasets [56–59]. The results of the cross-identification analysis are presented in Appendices B and C.

*a) Cross-identification with infrared catalogs*

To independently validate our classification and assess the novelty of the resulting sample, we performed a cross-identification of all 145 YSO candidates with the infrared catalogs presented in [20], where deep near-infrared (NIR) mapping of the W40–Serpens South region was carried out using CFHT observations combined with data from the 2MASS, UKIDSS and *Spitzer* surveys, resulting in a cleaned catalog containing 901,910 point sources. It is important to emphasize that the data presented in [20] were obtained using an independent methodology based on deep NIR and *Spitzer* observations and do not include WISE photometry, which forms the basis of the classification adopted in the present work. This makes the cross-comparison particularly valuable for an objective assessment of the reliability of our sample. The positional cross-identification shows that 137 out of 145 YSO candidates (94.5%) have counterparts in the general catalog presented in [20]. The highest completeness is achieved for the more evolved populations (Class II, Class III and transition disks), which is expected because of their enhanced brightness in the near-infrared wavelength range. A key result, however, is that comparison with the final sample of 832 verified YSOs identified in [20] shows that 124 out of our 145 candidates (85.5%) are absent from their final YSO catalog. Particularly notable are the results for the later evolutionary classes: 97.9% of the Class III objects and 100% of the transition-disk objects were not classified as YSOs in [20], indicating a substantial degree of novelty within the resulting sample. At the same time, it should be noted that a significant fraction of these sources had previously been identified in other studies of the Serpens South region based on X-ray, infrared and submillimeter observations. As an additional verification step, the 2MASS photometry of our objects was compared with the catalog data reported in [20], confirming the reliability of the source identifications (see Appendix B for details).

Since the infrared wavelength range provides the dominant contribution to the identification of young stellar objects in the studied region, additional data from several independent infrared surveys and specialized YSO catalogs were incorporated into the analysis

First, data from the *Spitzer*, WISE and NEOWISE space missions were used. The *Spitzer* survey (IRAC and MIPS) provides deep mid-infrared coverage in the 3.6–24 μm range, which is critically important for detecting circumstellar disks and protostellar objects, whereas WISE and its extension NEOWISE (3.4–22 μm) provide complete coverage of the entire region over a wider field of view, although with lower sensitivity compared to *Spitzer*. The combination of these surveys enables reliable identification of sources exhibiting infrared excess emission associated with accretion disks and dusty envelopes.

Second, several specialized YSO catalogs were employed. The MIRES (*Mid-InfraRed Excess Sources*) catalog presented in [60] was developed for the identification of massive young stellar objects and protostars using *Spitzer*/IRAC observations. In addition, the *Spitzer* YSO SED catalog provides a systematic classification of sources based on spectral energy distribution (SED) modeling in 22 star-forming regions, including Serpens South and represents one of the most widely used resources for identifying circumstellar disk systems.

Third, results from several independent studies were incorporated into the analysis. A combined analysis of infrared and X-ray observations in the Serpens South region revealed a significant number of YSO candidates. A machine-learning approach for YSO classification based on WISE data was developed in [61], while an updated catalog of young stellar objects was presented in [62]. In addition, YSO candidates in the Serpens–Aquila Rift complex were identified using a combination of WISE, 2MASS and Gaia observations.

Taken together, the combined use of these datasets showed that 114 out of 145 objects (78.6% of the sample) possess independent infrared confirmation of their YSO nature. Such a high fraction is expected because infrared wavelengths, particularly in the mid- and far-infrared ranges, penetrate the parental molecular clouds that strongly absorb optical and ultraviolet radiation. Moreover, infrared excess emission is a direct indicator of circumstellar disks and dusty envelopes, making infrared observations the primary and in many cases the only, method for identifying young stellar objects at early evolutionary stages. The obtained results confirm that the infrared wavelength range remains the principal tool for identifying protostellar and disk-bearing systems in the Serpens South region and further demonstrate the high reliability of the present sample, since the overwhelming majority of the candidates possess independent infrared confirmation from multiple datasets.

*b) ross-identification with radio and X-ray catalogs*

To independently verify the young nature of the sample of 145 YSO candidates, a cross-identification analysis was performed using radio and X-ray catalogs, as well as independent source catalogs associated with star-forming regions (the results are presented in Appendices B and C).

A comparison with the VLA Gould's Belt Survey (GBS) radio catalog, containing 146 sources detected at 4.5 GHz with a sensitivity of 10–15 μJy, revealed no positional matches within a search radius of 30″.

Despite the absence of direct matches with the VLA catalog, three objects in our sample possess independent confirmation in the radio and submillimeter wavelength ranges based on specialized studies of the Serpens South region. Previous molecular and radio investigations of the Aquila Rift complex have revealed dense molecular condensations, selective CO dissociation regions and complex gas kinematics associated with active star formation [63-65]. A catalog of millimeter and submillimeter sources in the W40–Serpens South region obtained with the JCMT telescope using the SCUBA-2 instrument (450 and 850 μm) revealed dense cold cores, many of which are associated with protostellar objects at early evolutionary stages. High-angular-resolution SMA observations further identified several compact millimeter sources corresponding to individual protostars and compact multiple systems in Serpens South. Recent interferometric studies of massive star-forming regions obtained with ALMA have additionally demonstrated the importance of molecular and ionized gas diagnostics for investigating the physical and dynamical properties of embedded young stellar environments [66-70]. Additional confirmation is provided by complementary catalogs of submillimeter and infrared-selected YSOs, as previously reported in [40, 62]. The catalog presented in [71] includes submillimeter and millimeter continuum sources identified in the Serpens South region using JCMT and IRAM 30m observations. The *Spitzer* YSO SED catalog additionally includes millimeter and radio detections for part of the sample, allowing these sources to be classified as protostellar objects with confirmed cold dust components. Based on these studies, three objects in our sample were identified as having radio or submillimeter confirmation: the first source was detected in the submillimeter range, as previously reported in [58, 62]; the second object was classified as a millimeter/radio source in [40]; and the third object was identified in the submillimeter range [71].

All three objects belong to the early evolutionary stages (Class I), which is expected because such sources possess the most massive and cold dusty envelopes emitting strongly in the submillimeter and millimeter wavelength ranges. The absence of matches with the VLA GBS catalog even for these three objects can be explained by differences in sensitivity and observing frequencies. The survey presented in [53] was carried out at 4.5 GHz (6 cm) and was optimized for the detection of free–free emission from ionized gas, whereas submillimeter observations in the 450–850 μm range are primarily sensitive to cold dust emission. Thus, these two observational regimes trace different physical components of protostellar systems (ionized winds/jets versus cold dusty envelopes) and are not necessarily expected to correlate directly.

The very small number of radio detections (≈2.1% of the total sample) is consistent with the results previously reported in [53], where only ~30% of YSOs in the Gould Belt were found to be detectable at radio wavelengths. Under the extreme conditions of the Serpens South region, this fraction may be even lower because of free–free absorption and the high optical depth of the surrounding medium.

Additional cross-identification with the MORX (*Million Optical Radio/X-ray Associations*) catalog did not reveal statistically significant matches within the investigated area (≈0.05 $deg^2$), which is likely explained by the high extinction and incomplete coverage by deep surveys.

In contrast, X-ray observations provide strong independent confirmation of the young nature of the sources, since high-energy emission is a direct indicator of magnetic activity characteristic of stars at early evolutionary stages. The principal contribution comes from two major catalogs. The first is the SFiNCs (*Star Formation in Nearby Clouds*) catalog, derived from a homogeneous analysis of archival *Chandra* X-ray and *Spitzer* infrared observations covering 22 star-forming regions [51]. This project identified more than 15,300 X-ray sources, nearly 8,500 of which were classified as probable young stellar members, increasing the known YSO populations in some regions by factors of 6%–200%.

The second dataset is a dedicated X-ray study of the Serpens South region, as previously reported in [52]. Using *Chandra* ACIS-I observations, that study identified 152 X-ray sources, of which 66 obtained reliable infrared counterparts based on *Spitzer* and 2MASS data, while 95 were classified as new YSO candidates.

Within our sample, 102 objects (70.3%) possess independent X-ray confirmation. This fraction demonstrates not merely a significant but rather a dominant overlap between the infrared- and X-ray-selected populations. The obtained value is fully consistent with the fundamental observational trends established for star-forming regions. Previous studies [63] have shown that the X-ray detection fraction of YSOs reaches approximately 70%–75% for more evolved objects, particularly Class II and Class III sources. Our results are therefore fully consistent with this established statistical behavior and confirm that the observed population represents a typical sample of young stars, for which X-ray activity serves as a reliable indicator of youth independent of the effects of dusty envelopes and circumstellar disks. The optical depth for soft X-ray emission (~0.5–8 keV) is substantially lower than at optical wavelengths, allowing the detection of sources deeply embedded within their parental molecular clouds.

Thus, the X-ray data not only complement but also independently validate the infrared classification. The high fraction of joint detections (infrared + X-ray) serves as a robust indicator that the identified sources represent a real and physically young stellar population rather than artifacts or erroneous identifications.

*c) Cross-identification with multiwavelength data*

An integrated assessment of the multiwavelength confirmations was performed in order to quantitatively evaluate the contribution of each wavelength range to the verification of the sample. Based on comparisons with infrared (*Spitzer*, WISE, NEOWISE and 2MASS), X-ray (SFiNCs and *Chandra*, as previously reported in [52]) and optical datasets, all 145 candidates were classified according to the type of observational confirmation.

Objects possessing exclusively infrared confirmation, without detections in the X-ray or optical wavelength ranges, account for 61 sources (42.1% of the sample). This category mainly includes highly obscured objects for which the X-ray emission may be significantly attenuated, as well as intrinsically faint X-ray sources lying below the sensitivity limits of the adopted surveys.

A total of 13 objects (9.0% of the sample) are detected only in X-rays without independent infrared confirmation. The presence of X-ray emission in the absence of detectable infrared excess may indicate several possible scenarios: (a) very low-mass objects such as ultracool dwarfs, (b) sources so strongly obscured in the infrared range that they are absent from the adopted catalogs, or (c) possible artifacts related to X-ray data processing. Additional spectral energy distribution (SED) analysis is required for the final classification of these objects.

Joint infrared and X-ray confirmation is observed for 28 objects (19.3% of the sample). Such sources represent highly reliable YSO candidates because two independent physical mechanisms – thermal emission from circumstellar dust and X-ray emission from magnetically active coronae – simultaneously indicate a young stellar nature. This category may therefore be considered the "gold standard" for cross-validation of YSO samples.

Optical data play a secondary role, providing confirmation for only 21 objects (14.5% of the sample). Such a low fraction is expected because of the extreme conditions in the Serpens South region: the high level of interstellar extinction typical of dense molecular clouds strongly suppresses optical emission, even in the I band (~800–900 nm). Consequently, optical detections are generally limited to the outermost and least obscured members of the association or to foreground objects.

Complete three-wavelength confirmation (infrared + X-ray + optical) is achieved for 21 objects (14.5% of the sample). These represent the most reliable YSO candidates, for which not only high-energy and dust-related emission but also optical radiation has been detected, primarily in red optical filters. This suggests comparatively low extinction along the line of sight or a location outside the densest regions of the molecular cloud.

Particular attention should be given to 11 objects (7.6% of the sample) that do not possess confirmation in any of the considered wavelength ranges (infrared, X-ray, or optical) (Table 4). A key result of the present study is the demonstration that all of these sources are present in the general point-source catalog presented in [20], which contains 901,910 reliable astronomical sources in the Serpens South region. Therefore, these objects represent real astrophysical sources rather than artifacts related to WISE data processing. Moreover, although these sources are included in the deep multiwavelength catalog reported in [20], they were not included in the final sample of 832 verified YSOs identified in that study. This discrepancy is likely explained by two factors. First, the methodology adopted in [20] relied primarily on deep NIR (CFHT) and *Spitzer* observations together with more restrictive selection criteria designed to minimize false identifications, potentially excluding fainter or more heavily obscured sources. Second, the present work makes extensive use of WISE photometry, which was not incorporated into the methodology of [20]. In particular, the W3 (12 μm) and W4 (22 μm) bands provide unique sensitivity to warm dust emission associated with circumstellar disks and dusty envelopes, enabling the identification of YSOs that may remain undetected in shorter-wavelength NIR observations. Thus, the WISE-based criteria adopted in the present study made it possible to identify a population of young objects that was not recovered using the more restrictive selection procedure of [20]. Collectively, these results emphasize the substantial novelty of the present study, in which these sources are identified for the first time as YSO candidates.

The absence of X-ray, optical and radio detections for these 11 objects, including Class I, II and III sources, does not contradict their young stellar nature. For Class II and III objects, this may be explained by several factors: (a) the large intrinsic spread in YSO X-ray luminosities, which may vary by up to two orders of magnitude within a single evolutionary class [72, 73], allowing weak sources to fall below the sensitivity limit of *Chandra* observations; (b) variability of magnetic activity analogous to solar flares; and (c) residual extinction attenuating soft X-ray emission. For Class I objects, an additional factor is the strong shielding produced by dense dusty envelopes.

The absence of optical detections is also expected. Even for Class III sources in Serpens South, the typical extinction reaches several magnitudes, rendering optical emission inaccessible to most ground-based surveys. Likewise, the absence of radio detections is not unusual, since only approximately 30% of YSOs in the Gould Belt are detectable at 4.5 GHz, as previously reported in [53].

Therefore, the absence of multiwavelength confirmations can be explained by a combination of factors, including low luminosity, variability, extinction and survey sensitivity limitations, rather than by the absence of a young stellar nature. These 11 objects represent valuable candidates for future deep observations. Additional observations with facilities such as ALMA, JCMT and NOEMA, together with detailed Herschel-based spectral energy distribution analysis are required for the final verification and classification of these sources.

Overall, the combined analysis presented here demonstrates the varying levels of reliability in YSO identification across the studied region and emphasizes the essential role of a multiwavelength approach, particularly for heavily obscured star-forming environments.

**Table 4.** New YSO candidates in the Serpens south region.

| *№* | *AllWISE* | *RA(J2000), deg* | *DE(J2000), deg* | *W1, mag* | *W2, mag* | *W3, mag* | *W4, mag* | *YSO Candidate (class)* |
|---|---|---|---|---|---|---|---|---|
| SS_YSO_01 | J183003.69-015842.5 | 277.52 | -01.98 | 15.877 | 13.835 | 10.513 | 8.120 | I |
| SS_YSO_02 | J183016.33-020149.3 | 277.57 | -02.03 | 15.210 | 13.840 | 9.555 | 7.049 | I |
| SS_YSO_03 | J183017.04-020409.5 | 277.57 | -02.07 | 15.548 | 13.280 | 10.075 | 7.338 | I |
| SS_YSO_04 | J183000.31-020616.0 | 277.50 | -02.10 | 14.222 | 12.732 | 10.414 | 4.829 | I |
| SS_YSO_05 | J183006.84-020806.8 | 277.53 | -02.14 | 14.243 | 12.207 | 10.120 | 8.193 | I |
| SS_YSO_06 | J183004.38-020539.0 | 277.52 | -02.09 | 14.050 | 12.936 | 10.799 | 8.580 | II |
| SS_YSO_07 | J182947.76-015941.6 | 277.45 | -01.99 | 13.132 | 12.588 | 10.866 | 8.631 | II |
| SS_YSO_08 | J183022.05-015921.5 | 277.59 | -01.99 | 13.266 | 12.547 | 9.367 | 6.740 | II |

*Continuation of the table*

| *№* | *AllWISE* | *RA(J2000), deg* | *DE(J2000), deg* | *W1, mag* | *W2, mag* | *W3, mag* | *W4, mag* | *YSO Candidate (class)* |
|---|---|---|---|---|---|---|---|---|
| SS_YSO_09 | J183017.84-020215.3 | 277.57 | -02.04 | 14.179 | 13.792 | 9.900 | 7.986 | III |
| SS_YSO_10 | J182942.40-020515.0 | 277.423 | -02.09 | 12.044 | 11.902 | 9.898 | 6.883 | III |
| SS_YSO_11 | J182937.64-020401.0 | 277.41 | -02.07 | 13.242 | 13.067 | 9.947 | 6.579 | III |

*4.4 Comparison with other star-forming regions and interpretation*

The results obtained in the present study allow a comparison between the Serpens South region and other well-studied star-forming environments, including NGC 1333, Ophiuchus, Serpens Core and IC 348.

1. A systematic comparison of five star-forming regions – Serpens South, Serpens Core, Ophiuchus, NGC 1333 and IC 348 — was previously presented in [74]. That study showed that, for most regions, the distribution of young stellar objects on scales larger than 0.15 pc is well described by the gas column density distribution, while the spatial distribution of YSOs at a given column density remains statistically random. However, Serpens South and NGC 1333 exhibit significant deviations from this behavior on smaller spatial scales (~0.15 pc), indicating that star formation in these two regions cannot be explained solely by gas column density. Instead, additional local processes, such as turbulence, magnetic fields, or dynamical interactions, likely play an important role.

Our analysis of the spatial distribution (Figures 3–5) fully supports this interpretation. Figure 3a shows that the youngest objects, including protostars and Class I sources, are concentrated toward the central region and coincide with the densest structures visible in the WISE 12 μm infrared map, whereas Figure 3b demonstrates that Class III objects exhibit a substantially more uniform distribution. Figure 4 presents the cumulative distribution functions (CDFs) of radial distances for different evolutionary classes, showing a systematic shift of the Class I distribution toward smaller radii compared with the Class II and III populations. In addition, Figure 5 shows the kernel density estimation (KDE) of the source distribution, where the contours associated with Class I objects demonstrate pronounced clustering, while the Class II population exhibits a significantly weaker concentration.

The quantitative estimates summarized in Table 2 show that the characteristic radius for Class I objects is $R_{50} = 0.26 \pm 0.03$ pc, whereas for Class II objects $R_{50} = 0.37 \pm 0.02$ pc. The median gas density derived from our Jeans analysis ($n \approx 1.6\times10^5$ см$^{-3}$; see Figure 6 and Table 3 in Section 3.3d) significantly exceeds the average density of typical molecular clouds (~$10^3$–$10^4$ см$^{-3}$) and corresponds to dense filamentary structures and prestellar cores detected with *Herschel*, as previously reported in [28, 36].

2. Comparison with the nearby W40 region provides important evolutionary information. According to the deep near-infrared survey presented in [20], the central region of W40 is dominated by Class II YSOs, corresponding to a more evolved stellar population, whereas approximately half of the YSOs in Serpens South belong to the younger Class I stage. This suggests that Serpens South is in an earlier stage of cluster evolution despite its spatial proximity and kinematic association with W40.

Our results are fully consistent with this interpretation. In the present sample, the fraction of Class I objects and protostars reaches approximately 26% (38 out of 145 objects). Furthermore, 124 out of 145 YSO candidates (85.5%) are absent from the final YSO catalog presented in [20], demonstrating the high efficiency of WISE data for identifying heavily obscured sources at early evolutionary stages.

3. The density estimates and clustering scales derived in this work can also be compared with those observed in other young embedded clusters. For example, in the NGC 1333 cluster, which also exhibits deviations from the model of on small spatial scales, the average gas density is approximately ~$10^5$ см$^{-3}$, nearly identical to our estimate for Serpens South ($n \approx 1.6\times10^5$ см$^{-3}$; see Table 3). By contrast, in more diffuse star-forming regions such as IC 348 and Taurus, the gas density is significantly lower and the spatial distribution of YSOs is more accurately described by the gas column density distribution without requiring additional local interactions.

The characteristic clustering scale obtained for Serpens South in the present study ($R_{50} = 0.26 \pm 0.03$ pc for Class I objects; see Table 2) is also consistent with the typical sizes of dense cores embedded within filamentary structures observed by *Herschel* as part of the Gould Belt Survey, as previously reported in [28, 36]. The mean nearest-neighbor distance for

Class I objects is 0.055 pc (Table 2), corresponding to typical fragmentation scales of dense molecular filaments.

4. A recent study [75] investigated the hierarchical structure of YSOs in the W40–Serpens South region using the minimum spanning tree (MST) method. The authors showed that the fractal dimensions in the central regions are approximately 1.6 for W40 and 1.4 for Serpens South. The lower fractal dimension derived for Serpens South indicates a higher degree of clustering, implying that the YSOs in Serpens South are concentrated into more compact groups.

Our analysis (see Figure 5 with KDE contours and Table 2 with the quantitative parameters) yields results fully consistent with this interpretation. Figure 3 shows that the youngest objects (Class I sources) exhibit the highest degree of spatial concentration, whereas Class II and III objects are distributed more uniformly throughout the region. The peak KDE density for the Class I population ($2.95\times10^{-5}$) is approximately three times higher than that of the Class II population ($1.05\times10^{-5}$), confirming a substantially stronger degree of clustering at earlier evolutionary stages. As previously reported in [20], four MST branches overlap with the main filament of Serpens South and molecular gas "hubs" together with an enhanced concentration of Class I YSOs are observed at their intersection points.

Thus, the comparison presented here, based on the quantitative results of our study (Figures 3–6 and Tables 1–3), allows the following conclusions to be drawn.

Serpens South, together with NGC 1333, belongs to the class of star-forming regions in which small-scale processes, including local interactions, turbulence and magnetic fields, play a key role in regulating star formation, distinguishing these environments from more diffuse regions such as IC 348 [76]. Our CDF distributions (Figure 4) and radial parameters (Table 1) quantitatively support this conclusion.

From an evolutionary perspective, Serpens South appears to be at an earlier stage of cluster evolution than the neighboring W40 region, as indicated by the high fraction of Class I objects identified both in our sample and in the catalog presented in [20].

The higher degree of clustering (corresponding to a lower fractal dimension) observed for the young population in Serpens South relative to other star-forming regions reflects the hierarchical structure of the dense filamentary cloud in which the stars are forming. Our KDE maps (Figure 5) and clustering parameters (Table 2) provide a quantitative basis for this interpretation.

## 5. Conclusion

In the present work, a comprehensive study of the young stellar object (YSO) population in the active star-forming region Serpens South, located within the Aquila Rift complex, has been carried out. Using multiwavelength data from the AllWISE catalog together with modern photometric selection criteria, a set of results was obtained that provides insight into the physical processes occurring within the region.

A representative sample of 145 YSO candidates was identified and classified according to their probable evolutionary stages. Protostellar candidates together with Class I objects account for approximately 26% of the sample, which, combined with the detected Class II population, suggests a high level of ongoing star formation activity. The presence of Class III candidates and transition disks further indicates a possible evolutionary sequence within the region, supporting the interpretation of Serpens South as one of the youngest nearby star-forming environments in the Galaxy.

The analysis of the spatial distribution of the sources indicates a likely correlation between evolutionary stage and the morphology of the surrounding gas. Early-stage objects exhibit clear spatial segregation and are preferentially concentrated along dense dusty filaments. In contrast, the more diffuse distribution of Class II and III objects may reflect dynamical relaxation processes and the gradual dispersal of the stellar population from the parental molecular structures.

A Jeans analysis combined with statistical modeling was used to estimate the local physical conditions within the fragmentation regions. The derived gas volume density, $n \approx 1.6 \times 10^5$ cm$^{-3}$, is consistent with theoretical models of star formation occurring within filamentary hubs and may support the important role of gravitational instability in this region.

The performed cross-identification with independent astrophysical catalogs, including *Chandra*/SFiNCs and *Spitzer* datasets, provides additional confirmation of the reliability of the adopted methodology. A substantial fraction of the sample exhibits both infrared excess emission and X-ray activity, characteristic of magnetically active young stellar objects.

During the course of this study, 11 new YSO candidates not previously reported in the literature were identified, including one potentially deeply embedded Class I source. These results suggest that WISE observations provide an efficient method for detecting objects located in regions of strong interstellar extinction that may remain inaccessible to near-infrared surveys.

Overall, the obtained results expand the current understanding of the star-forming architecture of the Serpens South region. The identified spatial structure together with the newly detected YSO candidates demonstrates the importance of further observational studies aimed at determining the detailed physical properties of individual members of this association.

**Funding**

This research was funded by the Science Committee of the Ministry of science and Higher Education of the Republic of Kazakhstan (Grant No. AP23489575).

**Conflicts of interest**

The authors declare no conflict of interest.

**Author contributions**

Conceptualization, N.Sh. and A.B.; Methodology, A.Zh.; Formal Analysis, N.Sh.; Investigation, N.E.; Data Curation, A.B. and N.B.; Visualization, K.M. and N.E.; Writing–Original Draft Preparation, A.Zh. and N.Sh.; Writing–Review and Editing, A.M., N.B., N.Sh., and A.Zh.; Validation, A.A., K.M., and A.B.; Supervision, N.Sh. and A.Zh. All authors have read and agreed to the published version of the manuscript.

**References**

1. G. Saral *et al.*, "Young Stellar Objects in the Massive Star-forming Regions W51 and W43," *The Astrophysical Journal*, vol. 839, no. 2, pp. 108–108, Apr. 2017, https://doi.org/10.3847/1538-4357/aa6575

2. M. W. Werner *et al.*, "The *Spitzer Space Telescope* Mission," *The Astrophysical Journal Supplement Series*, vol. 154, no. 1, pp. 1–9, Sep. 2004, doi: https://doi.org/10.1086/422992

3. E. L. Wright *et al.*, "The wide-field infrared survey explorer (wise): mission description and initial on-orbit performance," *The Astronomical Journal*, vol. 140, no. 6, pp. 1868–1881, Nov. 2010, doi: https://doi.org/10.1088/0004-6256/140/6/1868

4. M. Sewiło *et al.*, "Identifying Young Stellar Objects in the Outer Galaxy: $l$ = 224° Region in Canis Major," *The Astrophysical Journal Supplement Series*, vol. 240, no. 2, pp. 26–26, Feb. 2019, https://doi.org/10.3847/1538-4365/aaf86f

5. A.B. Manapbayeva, J. Esimbek, N.Sh. Alimgazinova, M.T. Kyzgarina, A.B. Atamurat, "Identification of Young Star Objects Near the Dust Bubble N22," *Academic Scientific Journal of Computer Science*, no. 3, pp. 96–105, 2021, https://doi.org/10.32014/2020.2518-1726.51

6. A. B. Nazar, N. Sh. Alimgazinova, M. T. Kyzgarina, A. M. Demessinova and A. B. Manapbayeva, "Identification of young star objects near dust bubble N10," *Recent Contributions to Physics*, vol. 83, no. 4, Dec. 2022, doi: https://doi.org/10.26577/rcph.2022.v83.i4.02

7. A. M. Alisher, "Search and identification of young stellar objects in infrared dust bubbles N19," *Recent Contributions to Physics*, vol. 86, no. 3, Sep. 2023, https://doi.org/10.26577/rcph.2023.v86.i3.02

8. N. Alimgazinova *et al.*, "Study of the N126 dust bubble in the infrared wavelength range," *Recent Contributions to Physics*, vol. 89, no. 2, pp. 19–26, 2024,https://doi.org/10.26577/rcph.2024v89i2-03

9. N. Sh. Alimgazinova, A. B. Manapbayeva, A. Z. Omar, A. M. Demessinova, K. Turekhanova and N. E. Abildayev, "Study of the W40 Star-Forming Region Based on Observations by the WISE Infrared Space Telescope," *Herald of the Kazakh-British Technical University*, vol. 23, no. 1, pp. 346–357, Mar. 2026, https://doi.org/10.55452/1998-6688-2026-23-1-346-357

10. S.-J. Kang, C. R. Kerton, M. Choi and M. Kang, "A Comparative Observational Study of YSO Classification in Four Small Star-forming H ii Regions," *The Astrophysical Journal*,vol.845,no.1,p.21,Aug.2017, https://doi.org/10.3847/1538-4357/aa7da3

11. S. T. Megeath *et al.*, "Initial Results from the Spitzer Young Stellar Cluster Survey," vol. 154, no. 1, pp. 367–373, Sep. 2004, https://doi.org/10.1086/422823

12. R. A. Gutermuth *et al.*, "The *Spitzer* Gould Belt Survey of Large Nearby Interstellar Clouds: Discovery of a Dense Embedded Cluster in the Serpens-Aquila Rift," *The Astrophysical Journal*, vol. 673, no. 2, pp. L151–L154, Jan. 2008, https://doi.org/10.1086/528710

13. X. Koenig, D. Leisawitz, D. J. Benford, L. M. Rebull, D. Padgett and R. J. Assef, "*Wide-Field Infrared Survey Explorer Observations of the Evolution of Massive Star-Forming Regions*," *The Astrophysical Journal*, vol. 744, no. 2, pp. 130–130, Dec. 2011, https://doi.org/10.1088/0004-637x/744/2/130

14. X. P. Koenig and D. T. Leisawitz, "A Classification Scheme for Young Stellar Objects Using the Wide-Field Infrared Survey Explorer AllWISE Catalog: Revealing Low-Density Star Formation in the Outer Galaxy", *The Astrophysical Journal*, vol. 791, no. 2, p. 131, Aug. 2014, https://doi.org/10.1088/0004-637x/791/2/131

15. C. J. Lada, "Star Formation: From OB Associations to Protostars," *Symposium - International Astronomical Union*, vol. 115, pp. 1–18, 1987, https://doi.org/10.1017/S0074180900094766

16. T. P. Robitaille, "A modular set of synthetic spectral energy distributions for young stellar objects," *Astronomy & Astrophysics*, vol. 600, p. A11, Mar. 2017, https://doi.org/10.1051/0004-6361/201425486

17. S. Bontemps *et al.*, "The*Herschel*first look at protostars in the Aquila rift," *Astronomy and Astrophysics*, vol. 518, pp. L85–L85, Jul. 2010, doi: https://doi.org/10.1051/0004-6361/201014661.

18. “VizieR,” *Unistra.fr*, 2021. https://vizier.cds.unistra.fr/viz-bin/VizieR-3?-source=II/368&-out.max=50&-out.form=HTML%20Table&-out.add=_ut.add=_RAJ (accessed May 06, 2026).

19. “VizieR,” *Unistra.fr*, 2017. https://vizier.cds.unistra.fr/viz-bin/VizieR-3?-source=VIII/106/hppsc070&-out.max=50&-out.form=HTML%20Table&-out.add=_r&-out.add=_RAJ (accessed May 06, 2026).

20. J. Sun *et al.*, “Deep near-infrared survey towards the W40 and Serpens South region in the Aquila Rift: A comprehensive catalogue of young stellar objects,” *Monthly Notices of the Royal Astronomical Society*, vol. 516, no. 4, pp. 5244–5257, Sep. 2022, doi: https://doi.org/10.1093/mnras/stac2191

21. F. Jansen *et al.*, “XMM-Newton observatory,” *Astronomy & Astrophysics*, vol. 365, no. 1, pp. L1–L6, Jan. 2001, doi: https://doi.org/10.1051/0004-6361:20000036

22. T. M. Dame, D. Hartmann and P. Thaddeus, “The Milky Way in Molecular Clouds: A New Complete CO Survey,” *The Astrophysical Journal*, vol. 547, no. 2, pp. 792–813, Feb. 2001, doi: https://doi.org/10.1086/318388

23. L. Prato, E. L. Rice and V. M. Dame, “Where are all the Young Stars in Aquila?,” arXiv e-prints, p. arXiv:0811.2842

24. S. Dzib, L. Loinard, A. J. Mioduszewski, A. F. Boden, L. F. Rodríguez and R. M. Torres, “Vlba determination of the distance to nearby star-forming regions. iv. a preliminary distance to the proto-herbig aebe star ec 95 in the serpens core,” *The Astrophysical Journal*, vol. 718, no. 2, pp. 610–619, Jul. 2010, https://doi.org/10.1088/0004-637x/718/2/610

25. G. N. Ortiz-León *et al.*, “The Gould’s Belt Distances Survey (GOBELINS). V. Distances and Kinematics of the Perseus Molecular Cloud,” vol. 865, no. 1, pp. 73–73, Aug. 2018, https://doi.org/10.3847/1538-4357/aada49

26. V. Straižys, K. Černis and S. Bartašiūtė, “Interstellar extinction in the area of the Serpens Cauda molecular cloud,” *Open Astronomy*, vol. 5, no. 1, Jan. 1996, https://doi.org/10.1515/astro-1996-0106

27. J. Knude and C. Fabricius, “Luminosity and Intrinsic Color Calibration of Main-Sequence Stars With 2Mass Photometry: All Sky Local Extinction,” *Open Astronomy*, vol. 12, no. 4, Dec. 2003, https://doi.org/10.1515/astro-2017-0073

28. A. Men’shchikov *et al.*, “Filamentary structures and compact objects in the Aquila and Polaris clouds observed by*Herschel,*” vol. 518, pp. L103–L103, Jul. 2010, doi: https://doi.org/10.1051/0004-6361/201014668.

29. J. Smith, A. Bentley, M. Castelaz, R. D. Gehrz, G. L. Grasdalen and J. A. Hackwell, “Infrared sources and excitation of the W40 complex,” *The Astrophysical Journal*, vol. 291, p. 571, Apr. 1985, https://doi.org/10.1086/163097

30. J. P. Vallee, “Behind the H II region Sharpless 217 - The envelope of the diffuse molecular cloud at G159.1 + 3.3,” *The Astronomical Journal*, vol. 94, p. 679, Sep. 1987, https://doi.org/10.1086/114505

31. Vallee, J. P., Guilloteau, S. and MacLeod, J. M., “The edge of a molecular cloud : obseravtions of millimetric 13CO and C18O transitions in W 40.”, Astronomy and Astrophysics, vol. 266, EDP, pp. 520–531, 1992.

32. M. A. Kuhn, E. D. Feigelson, B. Reipurth, S. A. Rodney and G. P. Garmire, “A*chandra*observation of the obscured star-forming complex W40,” *The Astrophysical journal*, vol. 725, no. 2, pp. 2485–2506, Dec. 2010, https://doi.org/10.1088/0004-637x/725/2/2485

33. G. N. Ortiz-León *et al.*, “The gould’s belt distances survey (gobelins). iii. the distance to the serpens/aquila molecular complex,” *The Astrophysical Journal*, vol. 834, no. 2, pp. 143–143, Jan. 2017, doi: https://doi.org/10.3847/1538-4357/834/2/143

34. Y. Su *et al.*, “Local Molecular Gas toward the Aquila Rift Region,” *The Astrophysical Journal*, vol. 893, no. 2, p. 91, Apr. 2020, https://doi.org/10.3847/1538-4357/ab7fff

35. F. Nakamura, K. Dobashi, T. Shimoikura, T. Tanaka and T. Onishi, “Wide-field $^{12}$CO ( ) and $^{13}$CO ( ) Observations toward the Aquila Rift and Serpens Molecular Cloud Complexes. I. Molecular Clouds and Their Physical Properties,” *The Astrophysical Journal*, vol. 837, no. 2, p. 154, Mar. 2017, https://doi.org/10.3847/1538-4357/aa5ea6

36. Ph. André *et al.*, “From filamentary clouds to prestellar cores to the stellar IMF: Initial highlights from the*Herschel*Gould Belt Survey,” *Astronomy and Astrophysics*, vol. 518, p. L102, Jul. 2010, https://doi.org/10.1051/0004-6361/201014666

37. “SIMBAD Astronomical Database - CDS (Strasbourg),” *simbad.cds.unistra.fr*. https://simbad.cds.unistra.fr/simbad/

38. R. M. Cutri et al., “2MASS All Sky Catalog of Point Sources,” NASA/IPAC Infrared Science Archive, 2003. Available: http://irsa.ipac.caltech.edu/applications/Gator/

39. S. T. Megeath *et al.*, “The *spitzer space telescope*survey of the orion a and b molecular clouds. II. The spatial distribution and demographics of dusty young stellar objects,” *The Astronomical Journal*, vol. 151, no. 1, p. 5, Dec. 2015, https://doi.org/10.3847/0004-6256/151/1/5

40. M. M. Dunham *et al.*, “Young stellar objects in the gould belt,” *The Astrophysical Journal Supplement Series*, vol. 220, no. 1, p. 11, Sep. 2015, https://doi.org/10.1088/0067-0049/220/1/11

41. N. J. Evans II *et al.*, “The Spitzer c2d Legacy Results: Star-Formation Rates and Efficiencies; Evolution and Lifetimes,” *The Astrophysical Journal Supplement Series*, vol. 181, pp. 321–350, Apr. 2009, https://doi.org/10.1088/0067-0049/181/2/321

42. W. M. Smart, “Textbook on Spherical Astronomy,” 6th ed., Cambridge University Press, 1977, https://doi.org/10.1017/CBO9780511628791

43. E. D. Feigelson and L. Sivakumar, “Modern Statistical Methods for Astronomy,” Jul. 2012, https://doi.org/10.1017/cbo9781139015653

44. B. Efron, “Bootstrap Methods: Another Look at the Jackknife,” *The Annals of Statistics*, vol. 7, no. 1, pp. 1–26, Jan. 1979, doi: https://doi.org/10.1214/aos/1176344552

45. B. W. Silverman, *Density Estimation for Statistics and Data Analysis*. Boston, MA: Springer US, 1986. https://doi.org/10.1007/978-1-4899-3324-9

46. V. Könyves *et al.*, “A census of dense cores in the Aquila cloud complex: SPIRE/PACS observations from theHerschelGould Belt survey,” *Astronomy & Astrophysics*, vol. 584, p. A91, Nov. 2015, https://doi.org/10.1051/0004-6361/201525861

47. D. Arzoumanian *et al.*, “Characterizing interstellar filaments with*Herschel*in IC 5146,” *Astronomy and Astrophysics*, vol. 529, pp. L6–L6, May 2011, doi: https://doi.org/10.1051/0004-6361/201116596

48. H. Kirk, P. C. Myers, T. L. Bourke, R. A. Gutermuth, A. Hedden and G. W. Wilson, “Filamentary accretion flows in the embedded serpens south protocluster,” *The Astrophysical Journal*, vol. 766, no. 2, pp. 115–115, Mar. 2013, doi: https://doi.org/10.1088/0004-637x/766/2/115

49. P. André et al., “From filamentary networks to dense cores in molecular clouds: Toward a new paradigm for star formation,” in Protostars and Planets VI, H. Beuther et al., Eds., University of Arizona Press, Tucson, 2014, pp. 27–51.

50. R. B. Larson, “Cloud fragmentation and stellar masses,” *Monthly Notices of the Royal Astronomical Society*, vol. 214, no. 3, pp. 379–398, Jun. 1985, https://doi.org/10.1093/mnras/214.3.379

51. K. V. Getman *et al.*, “Star Formation In Nearby Clouds (SFiNCs): X-Ray and Infrared Source Catalogs and Membership,” *The Astrophysical Journal Supplement Series*, vol. 229, no. 2, pp. 28–28, Mar. 2017, https://doi.org/10.3847/1538-4365/229/2/28

52. E. Winston, S. J. Wolk, R. Gutermuth and T. L. Bourke, “Chandra Detection of an Evolved Population of Young Stars in Serpens South,” *The Astronomical Journal*, vol. 155, no. 6, p. 241, May 2018, doi: https://doi.org/10.3847/1538-3881/aabe82

53. G. N. Ortiz-León *et al.*, “The gould’s belt very large array survey. ii. the serpens region,” *The Astrophysical Journal*, vol. 805, no. 1, p. 9, May 2015, https://doi.org/10.1088/0004-637x/805/1/9

54. C. P. Gutiérrez *et al.*, “Supernova 2010ev: A reddened high velocity gradient type Ia supernova,” *Astronomy & Astrophysics*, vol. 590, p. A5, Apr. 2016, https://doi.org/10.1051/0004-6361/201527228

55. J. S. Urquhart *et al.*, “The Red MSX Source survey: distribution and properties of a sample of massive young stars,” *Monthly Notices of the Royal Astronomical Society*, vol. 410, no. 2, pp. 1237–1250, Sep. 2010, https://doi.org/10.1111/j.1365-2966.2010.17514.x

56. S. J. Wolk *et al.*, “YSOVAR: Mid-infrared Variability among YSOs in the Star Formation Region Serpens South,” *The Astronomical Journal*, vol. 155, no. 2, p. 99, Feb. 2018, https://doi.org/10.3847/1538-3881/aaa6c4

57. C. Ricci *et al.*, “BASS XXXVII: The Role of Radiative Feedback in the Growth and Obscuration Properties of Nearby Supermassive Black Holes,” *The Astrophysical Journal*, vol. 938, no. 1, pp. 67–67, Oct. 2022, https://doi.org/10.3847/1538-4357/ac8e67

58. M. Zhang *et al.*, “A deep near-infrared survey toward the aquila molecular cloud. i. molecular hydrogen outflows,” *The Astrophysical Journal Supplement Series*, vol. 219, no. 2, p. 21, Aug. 2015, https://doi.org/10.1088/0067-0049/219/2/21

59. W. Park *et al.*, “Quantifying Variability of Young Stellar Objects in the Mid-infrared Over 6 Years with the Near-Earth Object Wide-field Infrared Survey Explorer,” *The Astrophysical Journal*, vol. 920, no. 2, p. 132, Oct. 2021, https://doi.org/10.3847/1538-4357/ac1745

60. M. S. Povich *et al.*, “THE MYStIX INFRARED-EXCESS SOURCE CATALOG,” *The Astrophysical Journal Supplement Series*, vol. 209, no. 2, pp. 31–31, Nov. 2013, https://doi.org/10.1088/0067-0049/209/2/31

61. M. Juvela and D. Tharakkal, “Fast fitting of spectral lines with Gaussian and hyperfine structure models,” *Astronomy & Astrophysics*, vol. 685, p. A164, May 2024, https://doi.org/10.1051/0004-6361/202349044

62. A. Pietarila and J. W. Harvey, “Ca II 854.2 nm BISECTORS AND CIRCUMFACULAR REGIONS,” *The Astrophysical Journal*, vol. 764, no. 2, p. 153, Feb. 2013, https://doi.org/10.1088/0004-637x/764/2/153

63. K. Tursun *et al.*, “Ammonia observations towards the Aquila Rift cloud complex,” *Astronomy & Astrophysics*, vol. 643, p. A178, Nov. 2020, https://doi.org/10.1051/0004-6361/202037659

64. T. Komesh *et al.*, “Studies of the distinct regions due to CO selective dissociation in the Aquila molecular cloud,” *Astronomy & Astrophysics*, vol. 644, p. A46, Dec. 2020, https://doi.org/10.1051/0004-6361/202038632

65. T. Komesh *et al.*, “$H_2CO$ and H110α Observations toward the Aquila Molecular Cloud,” *The Astrophysical Journal*, vol. 874, no. 2, p. 172, Apr. 2019, https://doi.org/10.3847/1538-4357/ab0ae3

66. T. Komesh *et al.*, “ALMA observations of the environments of G333.0162+00.7615,” *Proceedings of the International Astronomical Union*, vol. 17, no. S373, pp. 35–38, Aug. 2021, https://doi.org/10.1017/s1743921323000121

67. A. A. Abdirakhman, A. Zh. Omar, N. Sh. Alimgazinova, D. R. Tuiakbayeva and D. Y. Baitursyn, “Identification of complex organic molecules in the hot molecular core G335.79+0.17,” *Eurasian Physical Technical Journal*, vol. 23, no. 1 (55), pp. 130–137, Mar. 2026, https://doi.org/10.31489/2025n2/130-137

68. A. Abdirakhman *et al.*, “Kinematics and structure of the massive star-forming region G350.29+0.12,” *Herald of the Kazakh-British Technical University*, vol. 23, no. 1, pp. 334–345, Mar. 2026, https://doi.org/10.55452/1998-6688-2026-23-1-334-345

69. Zh. Assembay *et al.*, “ALMA observations of the environments of G301.1364-00.2249A,” *Proceedings of the International Astronomical Union*, vol. 18, no. S380, pp. 204–206, Dec. 2022, https://doi.org/10.1017/s1743921323002624

70. A. Omar *et al.*, “ALMA Observations of G333.6-0.2: Molecular and Ionized Gas Environment,” *Galaxies*, vol. 13, no. 4, p. 73, Jun. 2025, https://doi.org/10.3390/galaxies13040073

71. S. Casanova, T. Montmerle, E. D. Feigelson and P. André, “ROSAT X-ray sources in the ρ Ophiuchi cloud core,” The Astrophysical Journal, vol. 439, p. 752, 1995, https://doi.org/10.1086/175211.

72. T. Preibisch *et al.*, “The Origin of T Tauri X-Ray Emission: New Insights from the *Chandra* Orion Ultradeep Project,” *The Astrophysical Journal Supplement Series*, vol. 160, no. 2, pp. 401–422, Oct. 2005, https://doi.org/10.1086/432891

73. E. D. Feigelson and T. Montmerle, “High-Energy Processes in Young Stellar Objects,” *Annual Review of Astronomy and Astrophysics*, vol. 37, no. 1, pp. 363–408, Sep. 1999, https://doi.org/10.1146/annurev.astro.37.1.363

74. J. Schaye and C. Dalla Vecchia, “On the relation between the Schmidt and Kennicutt-Schmidt star formation laws and its implications for numerical simulations,” *Monthly Notices of the Royal Astronomical Society*, vol. 383, no. 3, pp. 1210–1222, Dec. 2007, https://doi.org/10.1111/j.1365-2966.2007.12639.x

75. K. V. Getman, E. D. Feigelson, L. Townsley, J. Bally, C. J. Lada and B. Reipurth, “*Chandra*Study of Young Stellar Objects in the NGC 1333 Star-forming Cloud,” *The Astrophysical Journal*, vol. 575, no. 1, pp. 354–377, Aug. 2002, https://doi.org/10.1086/341219

76. J. Sun, R. A. Gutermuth, H. Wang, S. Zhang and M. Long, "Hierarchical structure of YSO clusters in the W40 and Serpens South region: group extraction and comparison with fractal clusters," *Monthly Notices of the Royal Astronomical Society*, vol. 516, no. 4, pp. 5258–5269, Sep. 2022, https://doi.org/10.1093/mnras/stac2362

77. Plunkett, S., Arce, H. G., Corder, S. A., Dunham, M. M., Garay, G., Mardones, D., & Bourke, T. L., The distribution of protostars in the Serpens South filamentary cluster. *Astronomy & Astrophysics*, 615, A9., 2018, https://doi.org/10.1051/0004-6361/201731945

78. Marton, G., Tóth, L. V., Zahorecz, S., & Molinari, S., The Herschel/PACS Point Source Catalogue. *Astronomy & Astrophysics,* 688, A203.,2024, https://doi.org/10.1051/0004-6361/202349044

79. van der Marel, N., Verhaar, B. W., van Terwisga, S., Merín, B., Herczeg, G. J., van Dishoeck, E. F., & Bouwman, J., A survey of transition disks in nearby star-forming regions. *Astronomy & Astrophysics,* 592, A126. 2016, https://doi.org/10.1051/0004-6361/201628073

80. Anderson, B., Dunham, M. M., Arce, H. G., Plunkett, S., & Mardones, D., ALMA observations of CO emission toward young stellar objects in the Serpens region. The Astrophysical Journal, 938, 55. 2022, https://doi.org/10.3847/1538-4357/ac8c2f

***Information about the authors:***

*Alimgazinova Nazgul – Candidate of Physical and Mathematical Sciences, Associate Professor, Department of Electronics and Astrophysics, Farabi University (Almaty, Kazakhstan, e-mail: nazgul.alimgazinova@kaznu.edu.kz).*

*Manapbayeva Arailym – PhD, Senior Lecturer, Department of Physics, Kazakh National Women's Teacher Training University (Almaty, Kazakhstan, e-mail: manapbayeva.arailym@gmail.com).*

*Omar Aruzhan (corresponding author) – PhD, Associate Professor-Researcher, Department of Electronics and Astrophysics, Farabi University (Almaty, Kazakhstan, e-mail: omar.aruzhan@kaznu.kz).*

*Turekhanova Kunduz – Candidate of Physical and Mathematical Sciences, Associate Professor-Researcher, Department of Plasma Physics, Nanotechnology and Computer Physics, Farabi University (Almaty, Kazakhstan, e-mail: kunduz@physics.kz).*

*Abildayev Nurlan – student, Department of Mathematics, Farabi University (Almaty, Kazakhstan, e-mail: nurlanabildaev833@gmail.com).*

*Demessinova Aizat – PhD, Senior Lecturer, Department of Electronics and Astrophysics, Farabi University (Almaty, Kazakhstan, e-mail: aizat.dem@gmail.com).*

*Alibek Akmaral – Senior Lecturer, Department of Physics, Kazakh National Women's Teacher Training University (Almaty, Kazakhstan, e-mail: alibek.akmaral@list.ru).*

*Shaimoldin Nurzhan – PhD student, State Key Laboratory of Radio Astronomy and Technology, Xinjiang Astronomical Observatory (Urumqi, China, e-mail: nurzhan@xao.ac.cn).*

## APPENDIX A
**Complete list of anomalous sources.**

**Table A1.** Candidate YSOs with anomalous color indices.

| AllWISE ID | RA (deg) | Dec (deg) | W1, mag | W2, mag | W3, mag | W1−W2, mag | W2−W3, mag | YSO |
|---|---|---|---|---|---|---|---|---|
| J183003.51−015647.0 | 18.500978 | −1.946338 | 12.561 | 9.569 | 11.027 | 2.992 | −1.458 | Protostar |
| J183010.76−015813.1 | 18.502991 | −1.970293 | 11.385 | 10.394 | 10.632 | 0.991 | −0.238 | Class III |
| J182936.66−015548.3 | 18.493519 | −1.930082 | 13.666 | 13.692 | 10.151 | −0.026 | 3.541 | Class III |

## APPENDIX B
**Cross-identification with the infrared catalog.**

Cross-identification with the infrared catalog previously reported in [20] was performed to independently verify our classification and assess the novelty of the obtained sample. The authors of [20] carried out deep near-infrared (NIR) mapping of the W40–Serpens South region using the CFHT (Canada–France–Hawaii Telescope) and combined these observations with data from the 2MASS, UKIDSS and *Spitzer* surveys. As a result, they produced a cleaned point-source catalog containing 901,910 reliable objects after applying strict artifact rejection procedures, including the removal of halos, false detections and lateral stripes. From this catalog, a sample of 832 verified young stellar objects (YSOs) of different evolutionary classes was identified.

It is important to emphasize that the data presented in [20] were obtained using an independent approach based on deep NIR and *Spitzer* observations and do not include WISE photometry, which forms the basis of our classification scheme. This makes the cross-comparison particularly valuable for an objective assessment of the reliability of our sample.

For each of the 145 YSO candidates identified in this work, we searched for positional counterparts in the catalog reported in [20]. A matching radius of 2″ was adopted, corresponding to the typical astrometric accuracy of the surveys considered. For every source in our sample, the angular distances to all objects in the comparison catalog were calculated and the closest source within the adopted radius was considered a counterpart.

The cross-identification with the full catalog of 901 910 sources demonstrated a high degree of positional agreement. Detailed statistics for the different object classes are presented in Table B1.

**Table B1.** Results of the cross-identification of YSO candidates with the full catalog.

| YSO Class | Total Number of Objects Identified in This Study | Found in the Catalog of [20] | Agreement (%) |
|---|---|---|---|
| Class I | 37 | 31 | 83.8 |
| Class II | 48 | 47 | 97.9 |
| Class III | 47 | 46 | 97.9 |
| Transition Disk | 12 | 12 | 100.0 |
| Protostars | 1 | 1 | 100.0 |
| Total | 145 | 137 | 94.5 |

n average, 94.5% of our candidates have positional counterparts in the independent deep NIR catalog previously reported in [20]. This strongly demonstrates that our sample consists of real astrophysical sources rather than artifacts or noise associated with WISE data processing. The highest matching completeness is achieved for the more evolved classes (Class II, Class III and Transition Disk), which is expected because these objects are brighter in the near-infrared wavelength range forming the basis of the catalog presented in [20].

Among the eight YSO candidates in our sample (5.5% of the total 145 sources) that were not found in the cleaned catalog of [20], seven objects possess independent confirmations in other astrophysical databases and published studies, indicating their genuine astrophysical nature despite the absence of cross-identification with the catalog of [20]. In particular, several objects have independent cross-identifications confirming their nature: J183000.62−020208.8 (Class I) is classified as a "confirmed Young Stellar Object" based on the 2MASS survey [39]; J183002.38−020356.9 (Class I) is identified as a "confirmed millimetric source (protostar)" [56]; the objects J183000.27−020356.1, J182952.35−015745.9 (Class I) and J183010.50−020307.6 (Class II) are confirmed as "Young Stellar Objects" in *Spitzer* surveys, whereas J183005.37−020746.5 (Class I) and J183008.32−015705.7 (Class III) are classified as "Young Stellar Object candidates" based on the same data [54]. All of these sources therefore possess independent cross-identifications in published catalogs, confirming their astrophysical reality.

The only object that was not found either in the catalog of [20] or in any other available published studies is WISE J183000.32−020616.0 (Class I) with coordinates α(J2000) =$18^h30^m00.316^s$ and δ(J2000)=−02°06′16.04″. Since it has not previously been reported either as a confirmed YSO or as a YSO candidate, we classify it as a new Class I young stellar object candidate, corresponding to the most deeply embedded and earliest evolutionary stage of star formation. This makes the source particularly valuable for future spectroscopic and multiwavelength investigations. Thus, our study not only confirms the existence of previously known sources omitted from the catalog of [20], but also reveals one genuinely new candidate, highlighting the advantage of the WISE-based classification method for identifying highly obscured protostellar objects.

For additional verification, we compared the 2MASS photometry of our objects with the measurements reported in the catalog of [20]. A match was considered confirmed when the photometric difference satisfied $\Delta m \leq 0.05$ mag in all three bands (J, H and K). The adopted threshold corresponds to a flux ratio of $F_1/F_2 \approx 0.955$ (a relative difference of 4.5%) and exceeds the typical photometric uncertainties ($\sigma \approx 0.01$–$0.03$ mag) by a factor of 2–5, corresponding to a significance level of approximately 1.7–5σ [39, 24]. Overall, 74.5% (102 out of 137) of the positionally matched sources passed the photometric consistency test. A clear dependence on evolutionary class is observed, ranging from 32.3% for heavily embedded Class I objects to 100% for Transition Disk sources with optically thin disks, further supporting the reliability of our classification scheme.

**Table B2.** 2MASS photometric confirmation for matched objects.

| YSO Class | Found in the Full Catalog of [20] | Good 2MASS Agreement | Fraction (%) |
|---|---|---|---|
| Class I | 31 | 10 | 32.3 |
| Class II | 47 | 38 | 80.9 |
| Class III | 46 | 42 | 91.3 |
| Transition Disk | 12 | 12 | 100.0 |
| Protostars | 1 | 0 | 0 |
| Total | 137 | 102 | 74.5 |

A key result of our study is the comparison with the sample of 832 YSOs previously reported in [20]. As shown in Table B3, 124 out of 145 of our candidates (85.5%) are not included in their final YSO list.

The results are particularly significant for the later evolutionary classes: 97.9% of the Class III objects and 100% of the Transition Disk sources were not classified as YSOs in the study of [20]. At the same time, it should be emphasized that, despite the absence of identification in that work, a substantial fraction of these sources has been independently detected and classified as young stellar objects in other catalogs and studies of the Serpens South region based on X-ray, infrared and submillimeter observations.

**Table B3.** Comparison of our sample with the verified YSOs of [20].

| YSO Class | Total Number of Objects Identified in This Study | Found in the YSO Sample | Unmatched Objects | Fraction of Unmatched Objects (%) |
|---|---|---|---|---|
| Class I | 37 | 14 | 23 | 62.2 |
| Class II | 48 | 5 | 43 | 89.6 |
| Class III | 47 | 1 | 46 | 97.9 |
| Transition Disk | 12 | 0 | 12 | 100.0 |
| Protostars | 1 | 1 | 0 | 0 |
| Total | 145 | 21 | 124 | 85.5 |

## APPENDIX C

**Table C1.** Identified YSOs in the Serpens south region.

| AllWISE | RA(J2000), deg | DE(J2000), deg | W1, mag | W2, mag | W3, mag | W4, mag | Observations | Reference | Catalog class |
|---|---|---|---|---|---|---|---|---|---|
| J183015.69-020720.5 | 277.57 | -02.12 | 13.589 | 12.040 | 11.091 | 4.335 | Sub-mm; IR | [53]; [58]; [20] | Protostar; YSO |
| J183001.27-020148.3 | 277.51 | -02.03 | 10.375 | 7.075 | 5.058 | 1.815 | IR; Sub-mm; X-ray | [80]; [58]; [79]; [20] | |
| J183004.44-020138.4 | 277.52 | -02.03 | 9.948 | 8.293 | 5.261 | 2.294 | IR; X-ray | [80]; [78]; [58]; [20] | |
| J183000.61-020208.8 | 277.50 | -02.04 | 11.289 | 9.346 | 7.179 | 3.195 | IR | [39]; [58] | YSO |
| J182959.03-020157.4 | 277.50 | -02.03 | 12.950 | 11.243 | 8.517 | 5.898 | IR; X-ray | [80]; [78]; [58]; [20] | Protostar; YSO |
| J183002.46-020258.0 | 277.51 | -02.05 | 8.532 | 6.383 | 4.366 | 1.443 | | [58]; [20] | |
| J183000.24-020052.5 | 277.50 | -02.02 | 14.877 | 12.286 | 10.184 | 5.866 | Sub-mm; X-ray; IR | [54]; [58];[20] | YSO |
| J182957.46-020240.3 | 277.49 | -02.05 | 14.917 | 13.639 | 10.750 | 8.562 | X-ray; IR | [78]; [58]; | |
| J183000.11-020026.3 | 277.50 | -02.00 | 14.378 | 13.036 | 9.908 | 6.905 | IR | [58] | YSO Cand. |
| J182957.05-020246.8 | 277.49 | -02.05 | 15.950 | 14.045 | 10.725 | 8.764 | | | YSO |
| J183001.30-020343.2 | 277.51 | -02.06 | 8.089 | 5.922 | 3.146 | 0.758 | IR; Sub-mm; X-ray | [60]; [54]; [58]; [64]; [20] | Protostar; YSO |
| J183000.26-020015.5 | 277.50 | -02.00 | 14.143 | 12.175 | 10.081 | 6.977 | IR; X-ray | [58]; [20] | YSO |
| J183002.37-020356.9 | 277.51 | -02.07 | 14.195 | 11.944 | 9.427 | 3.921 | IR; Radio | [77]; [40] | Protostar; Millimetric Radio Source |
| J183000.27-020356.1 | 277.50 | -02.07 | 14.471 | 12.295 | 9.280 | 4.061 | IR | [54] ; [58] | YSO |
| J183006.29-015941.1 | 277.53 | -01.99 | 14.300 | 13.060 | 10.719 | 8.106 | X-ray | [78]; [58] | |
| J183002.64-020426.4 | 277.51 | -02.07 | 15.820 | 13.192 | 10.833 | 8.433 | IR; X-ray | [58] | ? |
| J183001.72-015907.7 | 277.51 | -01.99 | 15.037 | 13.515 | 10.848 | 8.200 | X-ray | | |
| J183014.20-020420.4 | 277.56 | -02.07 | 15.785 | 14.098 | 10.646 | 7.930 | IR | [58] | YSO |
| J183010.09-020537.4 | 277.54 | -02.09 | 15.286 | 13.434 | 10.460 | 7.760 | X-ray | | ? |
| J182954.36-015823.5 | 277.48 | -01.97 | 14.580 | 11.806 | 9.785 | 6.930 | IR; X-ray | [58]; [20] | YSO |

*Continuation of the table*

| AllWISE | RA(J2000), deg | DE(J2000), deg | W1, mag | W2, mag | W3, mag | W4, mag | Observations | Reference | Catalog class |
|---|---|---|---|---|---|---|---|---|---|
| J183001.09-020608.9 | 277.50 | -02.10 | 11.143 | 9.365 | 7.217 | 3.304 | IR; Sub-mm; X-ray | [40]; [58];[20] | Protostar; YSO |
| J183017.43-015948.2 | 277.57 | -01.99 | 15.352 | 14.567 | 10.962 | 8.218 | X-ray | [58] | ? |
| J182953.81-015748.3 | 277.47 | -01.96 | 11.899 | 10.078 | 8.023 | 5.580 | IR | [20] | YSO |
| J183000.08-015715.7 | 277.50 | -01.95 | 12.301 | 10.519 | 7.818 | 5.033 | IR; Sub-mm; X-ray | [78]; [20] [54]; [58] | Protostar; YSO |
| J183009.87-020633.7 | 277.54 | -02.11 | 14.770 | 13.844 | 10.656 | 8.055 | X-ray | [78]; [58] | |
| J182952.34-015745.9 | 277.47 | -01.96 | 16.256 | 12.537 | 10.286 | 6.066 | IR; X-ray | [54]; [58]; [20] | YSO |
| J182953.87-015727.9 | 277.47 | -01.96 | 13.774 | 12.409 | 10.143 | 7.295 | IR | | |
| J183021.54-020412.7 | 277.59 | -02.07 | 13.871 | 12.588 | 10.299 | 7.317 | X-ray | [54]; [58] | ? |
| J183005.37-020746.5 | 277.52 | -02.13 | 14.724 | 12.447 | 10.296 | 8.378 | IR | | YSO Cand. |
| J183025.45-020423.9 | 277.61 | -02.07 | 14.382 | 12.805 | 9.317 | 6.774 | X-ray | | ? |
| J183003.14-020514.8 | 277.51 | -02.09 | 11.421 | 10.472 | 9.147 | 6.491 | Sub-mm; X-ray | [78]; [58]; [20] | |
| J182943.00-020317.1 | 277.43 | -02.05 | 10.437 | 9.496 | 8.206 | 6.984 | IR; X-ray | [58]; [20] | |
| J183002.99-020717.9 | 277.51 | -02.12 | 12.770 | 11.892 | 10.701 | 8.453 | X-ray | [78]; [58] | |
| J182956.75-020233.1 | 277.49 | -02.04 | 14.467 | 13.761 | 10.771 | 8.743 | X-ray; IR | [53]; [58] | |
| J182959.07-020030.0 | 277.49 | -02.00 | 12.929 | 11.918 | 9.345 | 6.760 | | | YSO |
| J183005.93-020017.3 | 277.52 | -02.00 | 13.232 | 12.192 | 10.190 | 7.759 | IR | [58] | |
| J183008.06-020018.1 | 277.53 | -02.01 | 14.104 | 13.443 | 10.686 | 8.348 | X-ray; IR | [53]; [58] | |
| J183008.55-020023.0 | 277.54 | -02.01 | 13.384 | 12.631 | 10.704 | 8.182 | | | |
| J183010.56-020305.3 | 277.54 | -02.05 | 13.375 | 12.560 | 10.909 | 7.628 | IR | [54]; [58] | |
| J183009.16-020007.3 | 277.54 | -02.00 | 12.133 | 11.454 | 10.411 | 8.370 | | | |
| J182953.54-020059.4 | 277.47 | -02.02 | 13.888 | 13.389 | 10.565 | 7.932 | X-ray; IR | [53]; [58] | |
| J183008.57-015936.6 | 277.54 | -01.99 | 12.459 | 11.927 | 10.530 | 8.557 | | | YSO Cand. |
| J182956.68-020419.6 | 277.49 | -02.07 | 10.864 | 10.510 | 9.328 | 7.298 | | | |

*Continuation of the table*

| AllWISE | RA(J2000), deg | DE(J2000), deg | W1, mag | W2, mag | W3, mag | W4, mag | Observations | Reference | Catalog class |
|---|---|---|---|---|---|---|---|---|---|
| J183007.22-015919.7 | 277.53 | -01.99 | 10.218 | 9.429 | 8.160 | 6.107 | IR; Sub-mm; X-ray | [53]; [54]; [58]; [20] | YSO |
| J182958.90-020458.0 | 277.49 | -02.08 | 13.253 | 12.613 | 10.971 | 8.394 | X-ray; IR | [53]; [58] | |
| J182952.80-015939.9 | 277.47 | -01.99 | 13.838 | 12.863 | 10.823 | 7.679 | X-ray | [53] | ? |
| J183014.03-020438.8 | 277.56 | -02.08 | 13.079 | 12.765 | 10.801 | 8.393 | | | |
| J183020.13-020149.5 | 277.58 | -02.03 | 11.345 | 10.970 | 8.518 | 6.011 | | | |
| J183003.55-020617.4 | 277.51 | -02.10 | 12.547 | 11.548 | 9.998 | 7.393 | | | |
| J182944.88-020156.5 | 277.44 | -02.03 | 13.051 | 12.524 | 10.838 | 8.443 | | | |
| J183019.50-015951.6 | 277.58 | -01.99 | 14.563 | 13.898 | 10.630 | 8.018 | | | |
| J183006.87-015722.6 | 277.53 | -01.96 | 11.791 | 11.478 | 9.940 | 7.702 | IR | [58] | YSO Cand. |
| J182946.36-015941.5 | 277.44 | -01.99 | 13.157 | 12.700 | 10.395 | 8.199 | X-ray | [53] | ? |
| J183019.97-015948.9 | 277.58 | -01.99 | 13.703 | 13.104 | 10.179 | 7.520 | | | |
| J183021.51-020356.8 | 277.59 | -02.07 | 13.477 | 12.770 | 10.237 | 8.003 | | | |
| J182954.05-015714.8 | 277.48 | -01.95 | 14.128 | 13.149 | 10.364 | 8.240 | X-ray; IR | [53]; [58] | YSO |
| J183021.76-020417.7 | 277.59 | -02.07 | 13.099 | 12.107 | 10.290 | 7.331 | X-ray | [53] | ? |
| J183020.65-020450.8 | 277.59 | -02.08 | 13.062 | 12.292 | 10.135 | 7.716 | | | |
| J183006.93-015631.7 | 277.53 | -01.94 | 11.967 | 11.354 | 9.553 | 7.236 | X-ray; IR | [53]; [54]; [20] | YSO |
| J183021.58-020501.1 | 277.59 | -02.08 | 13.585 | 13.026 | 10.159 | 7.563 | X-ray | [53] | ? |
| J183016.98-020621.4 | 277.57 | -02.11 | 11.718 | 11.183 | 9.272 | 6.180 | X-ray; IR | [53]; [58] | YSO |
| J183006.79-020736.6 | 277.53 | -02.13 | 13.919 | 12.748 | 10.555 | 8.412 | IR | [58] | |
| J182939.61-020241.7 | 277.42 | -02.04 | 11.620 | 10.975 | 9.055 | 6.534 | X-ray; IR; Sub-mm | [53]; [78]; [54]; [79]; [20] | Disk; YSO |
| J182952.69-015639.0 | 277.47 | -01.94 | 13.396 | 12.734 | 10.368 | 8.168 | X-ray; IR | [53]; [58] | YSO Cand. |
| J183026.76-020143.5 | 277.61 | -02.03 | 11.274 | 10.963 | 9.213 | 6.762 | X-ray | [53] | ? |

*Continuation of the table*

| AllWISE | RA(J2000), deg | DE(J2000), deg | W1, mag | W2, mag | W3, mag | W4, mag | Observations | Reference | Catalog class |
|---|---|---|---|---|---|---|---|---|---|
| J183007.39-020753.3 | 277.53 | -02.13 | 14.040 | 12.919 | 10.615 | 8.226 | X-ray; IR | [53]; [58] | YSO Cand. |
| J182958.68-015600.9 | 277.49 | -01.93 | 13.942 | 12.983 | 10.914 | 8.695 | | | |
| J182959.28-015552.0 | 277.49 | -01.93 | 13.921 | 13.033 | 10.488 | 8.525 | | | YSO |
| J183007.11-020816.9 | 277.53 | -02.14 | 13.597 | 12.629 | 10.155 | 8.200 | IR | [58] | |
| J183022.78-020616.9 | 277.59 | -02.10 | 13.652 | 13.112 | 10.930 | 8.402 | X-ray | [53] | ? |
| J183001.60-015519.3 | 277.51 | -01.92 | 13.365 | 13.003 | 10.978 | 8.881 | X-ray; IR | [53]; [58] | YSO |
| J182936.98-020325.6 | 277.40 | -02.06 | 10.914 | 10.270 | 9.049 | 6.735 | | [53]; [54]; [20] | |
| J182953.74-020819.0 | 277.47 | -02.14 | 13.017 | 12.420 | 10.336 | 7.944 | X-ray | [53] | ? |
| J182957.56-015520.6 | 277.49 | -01.92 | 13.257 | 12.489 | 10.540 | 8.459 | X-ray; IR | [53]; [58] | YSO |
| J182943.12-020638.7 | 277.43 | -02.11 | 11.975 | 11.668 | 10.340 | 7.200 | X-ray | [53] | ? |
| J183024.31-020623.0 | 277.60 | -02.11 | 13.527 | 12.812 | 9.701 | 6.960 | X-ray; IR | [53]; [58];[20] | YSO |
| J182944.56-015644.5 | 277.44 | -01.95 | 13.267 | 12.650 | 9.380 | 5.291 | X-ray | [53] | ? |
| J183008.55-020619.0 | 277.54 | -02.11 | 11.278 | 10.838 | 9.815 | 7.433 | X-ray; IR | [53]; [58] | YSO Cand. |
| J182954.67-020410.4 | 277.48 | -02.07 | 10.404 | 9.918 | 9.638 | 7.730 | | | |
| J183016.81-020017.0 | 277.57 | -02.00 | 11.484 | 10.977 | 10.411 | 8.018 | X-ray | [53]; | ? |
| J182944.37-020035.0 | 277.44 | -02.01 | 11.026 | 10.669 | 10.350 | 8.014 | | | |
| J182941.61-020041.4 | 277.42 | -02.01 | 11.074 | 10.918 | 9.950 | 7.120 | | | |
| J182939.79-020302.3 | 277.42 | -02.05 | 12.242 | 11.939 | 10.793 | 8.499 | | [53]; [54]; | YSO |
| J182945.16-020612.8 | 277.44 | -02.10 | 10.709 | 10.423 | 9.494 | 7.286 | | [53]; | ? |
| J182951.06-020722.0 | 277.46 | -02.12 | 11.704 | 11.110 | 10.625 | 8.435 | | | |
| J183001.34-015547.7 | 277.51 | -01.93 | 11.606 | 11.281 | 10.506 | 8.558 | X-ray; IR | [53]; [58] | YSO Cand. |
| J183005.22-015544.5 | 277.52 | -01.93 | 11.982 | 11.754 | 10.765 | 8.588 | | | |
| J183008.79-020804.0 | 277.54 | -02.13 | 10.676 | 10.368 | 9.431 | 6.968 | | | |
| J183028.69-020253.0 | 277.62 | -02.05 | 10.583 | 10.335 | 9.307 | 7.340 | X-ray | [53]; | ? |
| J183029.70-020318.2 | 277.62 | -02.06 | 10.981 | 10.801 | 10.096 | 7.660 | | | |

*Continuation of the table*

| AllWISE | RA(J2000), deg | DE(J2000), deg | W1, mag | W2, mag | W3, mag | W4, mag | Observations | Reference | Catalog class |
|---|---|---|---|---|---|---|---|---|---|
| J182958.86-020245.7 | 277.49 | -02.05 | 11.345 | 11.257 | 10.884 | 8.593 | X-ray; IR | [53]; [58] | YSO |
| J183005.54-020307.6 | 277.52 | -02.05 | 12.113 | 11.999 | 10.843 | 7.156 | IR | [58] | |
| J183007.17-020301.0 | 277.53 | -02.05 | 8.330 | 7.779 | 7.721 | 6.854 | X-ray; IR | [53]; [58] | YSO Cand. |
| J183008.43-020306.4 | 277.54 | -02.05 | 8.797 | 8.096 | 7.927 | 7.472 | | | |
| J182956.36-020338.9 | 277.48 | -02.06 | 13.965 | 13.894 | 9.588 | 7.204 | | | |
| J183007.35-020415.5 | 277.53 | -02.07 | 13.999 | 13.811 | 9.969 | 7.434 | | | YSO |
| J182955.61-020346.3 | 277.48 | -02.06 | 14.197 | 14.113 | 10.491 | 8.283 | | | YSO Cand. |
| J182952.99-020101.5 | 277.47 | -02.02 | 13.744 | 13.430 | 10.197 | 7.531 | | | |
| J183013.86-020108.1 | 277.56 | -02.02 | 13.689 | 13.218 | 10.069 | 7.279 | | | |
| J183009.86-020420.8 | 277.54 | -02.07 | 9.687 | 8.942 | 8.599 | 7.652 | | | |
| J183015.01-020143.2 | 277.56 | -02.03 | 13.576 | 13.531 | 9.245 | 7.005 | X-ray | [53] | ? |
| J183015.34-020222.9 | 277.56 | -02.04 | 13.723 | 13.464 | 10.884 | 8.141 | | | |
| J183015.01-020306.9 | 277.56 | -02.05 | 13.493 | 13.322 | 9.908 | 7.343 | | | |
| J183009.14-020508.2 | 277.54 | -02.09 | 13.692 | 13.190 | 9.278 | 7.014 | | | |
| J183016.08-020322.6 | 277.57 | -02.06 | 13.891 | 13.506 | 10.360 | 7.336 | | | |
| J183017.68-020221.7 | 277.57 | -02.04 | 13.901 | 13.592 | 10.409 | 8.233 | | | |
| J183001.97-020557.8 | 277.51 | -02.10 | 11.367 | 11.243 | 10.706 | 5.584 | | | |
| J183004.89-015740.4 | 277.52 | -01.96 | 13.872 | 13.427 | 10.171 | 8.206 | X-ray; IR | [53]; [58] | YSO Cand. |
| J183016.42-015904.1 | 277.57 | -01.98 | 14.044 | 13.577 | 10.242 | 7.824 | | [54]; [20] | YSO |
| J183014.96-020528.6 | 277.56 | -02.09 | 13.650 | 13.473 | 9.667 | 7.044 | X-ray | [53] | ? |
| J183021.42-020103.4 | 277.59 | -02.02 | 13.878 | 13.503 | 9.582 | 6.674 | | | |
| J183008.21-015722.5 | 277.53 | -01.96 | 14.272 | 13.905 | 10.593 | 8.384 | IR | [58] | YSO Cand. |
| J183016.60-020520.6 | 277.57 | -02.09 | 13.685 | 13.534 | 9.225 | 7.051 | X-ray | [53] | ? |
| J183021.48-020025.8 | 277.59 | -02.01 | 14.001 | 13.592 | 10.575 | 8.337 | | | |
| J183023.03-020235.8 | 277.59 | -02.04 | 14.217 | 13.805 | 9.581 | 7.227 | | | |

*Continuation of the table*

| AllWISE | RA(J2000), deg | DE(J2000), deg | W1, mag | W2, mag | W3, mag | W4, mag | Observations | Reference | Catalog class |
|---|---|---|---|---|---|---|---|---|---|
| J183002.50-015655.5 | 277.51 | -01.95 | 13.760 | 13.559 | 9.658 | 7.690 | X-ray; IR | [53]; [58] | |
| J183008.22-015705.7 | 277.53 | -01.95 | 13.243 | 13.002 | 10.329 | 8.235 | IR | [54] ; [58] | YSO Cand. |
| J183011.59-015721.4 | 277.55 | -01.96 | 14.244 | 13.879 | 10.832 | 8.306 | X-ray; IR | [53]; [58] | |
| J183017.77-020531.6 | 277.57 | -02.09 | 14.312 | 14.103 | 9.712 | 6.861 | X-ray | [53] | ? |
| J183016.18-020601.1 | 277.57 | -02.10 | 13.289 | 12.943 | 9.357 | 6.379 | X-ray; IR | [53]; [58] | YSO Cand. |
| J183015.06-015732.9 | 277.56 | -01.96 | 13.951 | 13.760 | 10.636 | 7.760 | | | |
| J183026.15-020202.4 | 277.61 | -02.03 | 14.243 | 13.923 | 9.589 | 7.091 | X-ray | [53] | ? |
| J182941.43-020433.7 | 277.42 | -02.08 | 11.705 | 11.592 | 10.815 | 8.267 | | | |
| J183019.17-020632.0 | 277.58 | -02.11 | 13.805 | 13.579 | 9.515 | 6.772 | X-ray; IR | [53]; [58] | YSO |
| J183020.37-020617.0 | 277.58 | -02.10 | 13.466 | 13.105 | 9.613 | 6.871 | | | |
| J183028.95-020232.3 | 277.62 | -02.04 | 13.250 | 13.023 | 9.636 | 7.158 | | | |
| J182939.58-020456.3 | 277.41 | -02.08 | 11.651 | 11.520 | 10.620 | 8.557 | | | |
| J183026.72-020459.0 | 277.61 | -02.08 | 13.689 | 13.049 | 9.606 | 7.654 | X-ray | [53] | ? |
| J183029.72-020202.4 | 277.62 | -02.03 | 13.742 | 13.726 | 9.412 | 7.414 | | | |
| J183029.70-020233.5 | 277.62 | -02.04 | 14.078 | 13.864 | 9.358 | 7.145 | | | |
| J182938.64-020446.7 | 277.41 | -02.08 | 10.963 | 10.877 | 9.864 | 7.682 | | | |
| J183022.25-015709.4 | 277.59 | -01.95 | 8.342 | 7.655 | 7.599 | 7.368 | X-ray; IR | [53]; [78];[40] | YSO Cand. |
| J183013.74-015535.6 | 277.56 | -01.93 | 13.527 | 13.444 | 10.567 | 8.066 | X-ray | [53] | ? |
| J183013.11-015529.1 | 277.55 | -01.92 | 13.115 | 12.907 | 10.708 | 8.417 | | | |